

1 **Ozone affected by a succession of four landfall typhoons in**  
2 **the Yangtze River Delta, China: major processes and health**  
3 **impacts**

4 Chenchao Zhan <sup>a,1</sup>, Min Xie <sup>a,\*</sup>, Chongwu Huang <sup>a,1</sup>, Jane Liu <sup>b,c</sup>, Tijian Wang <sup>a</sup>, Meng Xu <sup>d</sup>, Chaoqun  
5 Ma <sup>a</sup>, Jianwei Yu <sup>e</sup>, Yumeng Jiao <sup>f</sup>, Mengmeng Li <sup>a</sup>, Shu Li <sup>a</sup>, Bingliang Zhuang <sup>a</sup>, Ming Zhao <sup>a</sup>,  
6 Dongyang Nie <sup>a</sup>

7 <sup>a</sup> School of Atmospheric Sciences, Joint Center for Atmospheric Radar Research of CMA/NJU,  
8 CMA-NJU Joint Laboratory for Climate Prediction Studies, Jiangsu Collaborative Innovation  
9 Center for Climate Change, Nanjing University, Nanjing 210023, China

10 <sup>b</sup> College of Geographic Sciences, Fujian Normal University, 350007, Fuzhou, China

11 <sup>c</sup> Department of Geography and Planning, University of Toronto, Toronto, Ontario, Canada

12 <sup>d</sup> Jiangsu Provincial Climate Center, Nanjing 210009, China

13 <sup>e</sup> Jiangsu Provincial Meteorological Observatory, Nanjing 210008, China

14 <sup>f</sup> Department of Microbiology and Parasitology, Bengbu Medical College, Bengbu 233030, China

15 -----

16 \* Corresponding author. minxie@nju.edu.cn (M. Xie)

17 <sup>1</sup> The third author can be considered as the co-first author

18

19 **Abstract:** Landfall typhoon can significantly affect O<sub>3</sub> in the Yangtze River Delta (YRD) region. In  
20 this study, we investigate a unique case characterized by two multiday regional O<sub>3</sub> pollution  
21 episodes related to four successive landfall typhoons in the summer of 2018 in the YRD. The results  
22 show that O<sub>3</sub> pollution episodes mainly occurred during the period from the end of a typhoon to the  
23 arrival of the next typhoon. The time when a typhoon reached the 24-h warning line and the time  
24 when the typhoon dies away in the mainland China can be roughly regarded as time nodes.  
25 Meanwhile, the variations of O<sub>3</sub> was related to the track, duration and landing intensity of the  
26 typhoons. The impact of typhoons on O<sub>3</sub> was like a wave superimposed on the background of high  
27 O<sub>3</sub> concentration in the YRD in summer. When a typhoon was near the 24-h warning line before it  
28 landed the coast line of the YRD, the prevailing wind originally from the ocean changed to from the  
29 inland, and transported lots of precursors from the polluted areas to the YRD. Under influences of  
30 the typhoon, the low temperature, strong upward airflows, more precipitation and wild wind

31 hindered occurrences of high O<sub>3</sub> episodes. After the passing of the typhoon, the air below the 700  
32 hPa atmospheric layer was warm and dry, and the downward airflows resumed. The low troposphere  
33 was filled with high concentration of O<sub>3</sub> due to O<sub>3</sub>-rich air transported from the low stratosphere and  
34 strong photochemical reactions. It is noteworthy that O<sub>3</sub> was mainly generated in the middle of  
35 boundary layer (~ 1000 m) instead of at the surface. High O<sub>3</sub> remained in the residual layer at night,  
36 and would be transported to the surface by downward airflows or turbulences by the second day.  
37 Moreover, O<sub>3</sub> can be accumulated and trapped on the ground due to the poor diffusion conditions  
38 because the vertical diffusion and horizontal diffusion were suppressed by downward airflows and  
39 light wind, respectively. The premature mortalities attributed to O<sub>3</sub> exposure in the YRD during the  
40 study period was 194.0, more than the casualties caused directly by the typhoons. This work has  
41 enhanced our understanding of how landfall typhoons affect O<sub>3</sub> in the YRD and thus can be useful  
42 to forecasting O<sub>3</sub> pollution in regions strongly influenced by typhoon activities.

43 **Key Words:** ozone; landfall typhoon; the Yangtze River Delta region;

44

## 45 **1 Introduction**

46 The tropospheric ozone (O<sub>3</sub>), which is formed by a series of complex photochemical reactions  
47 between volatile organic compounds (VOCs) and nitrogen oxides (NO<sub>x</sub>=NO+NO<sub>2</sub>) in combination  
48 with sunlight (Chameides and Walker, 1973; Xie et al., 2014), has received continuous attention due  
49 to its negative impact on air quality (Chan and Yao, 2008; Monks et al., 2015), human health (Jerrett  
50 et al., 2009), climate (Allen et al., 2012; IPCC, 2014) and biosphere (Dingenen et al., 2009).  
51 Research on urban O<sub>3</sub> pollution can be dated back to the early 1950s, beginning with the Los Angeles  
52 smog. In China, the photochemical smog, which is characterized by high level of O<sub>3</sub>, was first  
53 discovered in Xigu district of Lanzhou in 1970s (Tang et al., 1989). However, with the key  
54 atmospheric environmental problem was coal-smoke pollution (such as acid rain) at that time (Wang  
55 et al., 2019), little systematic research and coordinated O<sub>3</sub> monitoring were performed in China until  
56 the mid-2000s (Wang et al., 2017).

57 Since the beginning of the 21st century, the complex air pollution, which is dominated by fine  
58 particulate matter (PM<sub>2.5</sub>, particles of 2.5 microns or less in aerodynamic diameter) and surface O<sub>3</sub>,  
59 has been ingrained in the megacities of China (Chan and Yao, 2008; Jin et al., 2016; Kan et al.,  
60 2012). Air pollution has evolved into a political and economic concern in China. Due to the strict



61 air pollution control since 2013, particle pollution has been greatly reduced, appearing a  
62 significantly decrease in sulfur dioxide (SO<sub>2</sub>), NO<sub>x</sub> and PM<sub>2.5</sub>. However, the concentrations of O<sub>3</sub>  
63 and VOCs have increased from 2013 to 2017 (Li et al., 2017), suggesting that more attention should  
64 be paid to controlling O<sub>3</sub> and VOCs in the future. Overall, the causes of air pollution in China are  
65 remaining challenges to confront, especially in understanding the sources, transport and dispersion  
66 processes, and chemical formation mechanisms of O<sub>3</sub> and its precursors (Ding et al., 2016; Guo et  
67 al., 2014; Huang et al., 2014).

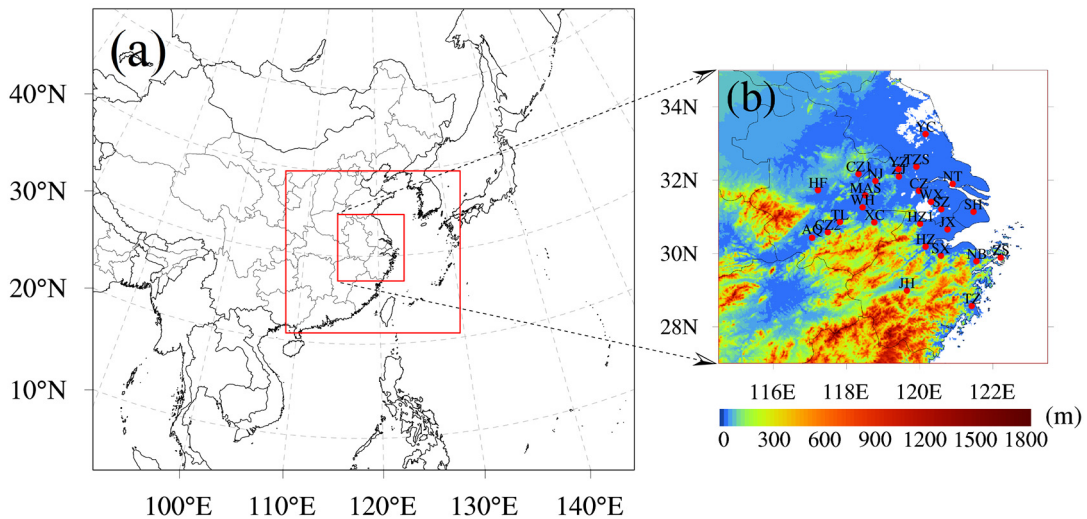
68 A typhoon (tropical cyclone, TC) is one of the most severe natural disasters in East Asia. Out  
69 of the total provinces in China, 10 coastal and 6 island provinces are affected by typhoon induced  
70 disasters, with more than 250 million lives are affected (Liu et al., 2009). The average number of  
71 typhoons making landfall in China is 9 each year, and those typhoons usually inflict vast losses in  
72 human life and property due to the accompanied strong wind, torrential rains and huge storm surges  
73 (Zhang et al., 2009; Zhao et al., 2012). Because of the long lifetime and tremendous energy,  
74 typhoons can significantly impact local atmospheric conditions, and thereby can affect surface O<sub>3</sub>  
75 concentration through advection, diffusion, deposition and other processes. The impact of typhoons  
76 on O<sub>3</sub> has attracted extensive attention in recent years (Deng et al., 2019; Huang et al., 2005; Jiang  
77 et al., 2015; Shu et al., 2016; Wang and Kwok, 2002; Wei et al., 2016; Yang et al., 2012). For  
78 example, Deng et al. (2019) reported that high O<sub>3</sub> and high aerosol concentrations (double high  
79 episodes) are likely to occur when the PRD is under the control of the typhoon periphery and the  
80 subtropical high with strong downdrafts. Previous studies were mainly in the southern China  
81 (including Hong Kong and Taiwan), where typhoons occur frequently. Still, research on the impact  
82 of landfall typhoons on O<sub>3</sub> is rather limited.

83 The Yangtze River Delta (YRD) region, being one of the most developed and densely  
84 populated regions in China, is located on the western coast of the Pacific Ocean. With 3.7% of the  
85 area and 16.0% of the population of China, the YRD contributed over 20% of the national total  
86 Gross Domestic Product (GDP) in 2019. Due to the rapid economic development and high energy  
87 consumption, this region has been suffering from intense air pollution (Ding et al., 2013; Li et al.,  
88 2019; Wang et al., 2015; Xie et al., 2016). In 2017, the 90th percentile of the maximum daily 8-hour  
89 average (MDA8) O<sub>3</sub> concentration was 170 µg m<sup>-3</sup>, and 16 of the 26 cities (Figure 1b) in the YRD  
90 failed to meet national standard ([http://www.cnemc.cn/jcbg/zghjzkgb/201905/t20190529\\_704755](http://www.cnemc.cn/jcbg/zghjzkgb/201905/t20190529_704755).

91 html). Therefore, it is urgent to investigate the spatiotemporal characteristic of O<sub>3</sub> as well as its  
 92 formation mechanisms in the YRD. Influenced by the monsoon weather, the warm and stagnation  
 93 conditions play an important role in the occurrence of high-level O<sub>3</sub> in summer (Li et al., 2018; Liao  
 94 et al., 2015; Lu et al., 2018; Zhao et al., 2010). Synoptic weather systems, such as typhoons and  
 95 cold fronts, can significantly impact O<sub>3</sub> in the YRD (Hu et al., 2013; Shu et al., 2016). This work  
 96 aims to reveal the main processes of landfall typhoon affecting surface O<sub>3</sub> in the YRD, to fill the  
 97 knowledge gap and thus provide scientific insight for effective pollution control measures.

98 In this study, we report a typical case observed in the YRD during the period from 16 July to  
 99 25 August, 2018, during which multiday episode of high O<sub>3</sub> occurred and was found to be related  
 100 to four successive landfall typhoons. Base on the monitoring data and numerical simulation, we  
 101 explore the impact of landfall typhoons on O<sub>3</sub> in the YRD, including the major processes and health  
 102 impacts. The following part of this paper is structured as the follows: Section 2 gives a brief  
 103 description of monitoring data, the analysis methods, and model configurations. The results as well  
 104 as the discussions are detailed in section 3. Section 4 summarizes the main conclusions.

105



106

107 **Figure 1. The three nested modeling domains (a) in WRF, and the locations of 26 cities in the**  
 108 **YRD with terrain elevation data (b). The cities in (b) include: Nanjing (NJ), Wuxi (WX),**  
 109 **Changzhou (CZ), Suzhou (SZ), Nantong (NT), Yancheng (YC), Yangzhou (YZ), Zhenjiang (ZJ)**  
 110 **and Taizhoushi (TZS) located in Jiangsu province; Hangzhou (HZ), Ningbo (NB), Jiaxing (JX),**  
 111 **Huzhou (HZ1), Shaoxing (SX), Jinhua (JH), Zhoushan (ZS) and Taizhou (TZ) located in**

112 Zhejiang province; Hefei (HF), Wuhu (WH), Maanshan (MAS), Tongling (TL), Anqing (AQ),  
113 Chuzhou (CZ1), Chizhou (CZ2) and Xuancheng (XC) located in Anhui province; and the  
114 megacity Shanghai (SH). The terrain elevation data are available at  
115 [https://www.ngdc.noaa.gov/mgg/global/relief/ETOPO1/data/bedrock/cell\\_registered/netcdf/](https://www.ngdc.noaa.gov/mgg/global/relief/ETOPO1/data/bedrock/cell_registered/netcdf/).

116

## 117 **2 Data and methods**

### 118 **2.1 Air quality data**

119 Surface air pollutants monitored by the China National Environmental Monitoring Center  
120 (CNMC) Network are used in this study. The nationwide observation network began operating in  
121 74 major cities in 2013, and it included 1597 nonrural sites covering 454 cities by 2017 (Lu et al.,  
122 2018). The monitoring data are strictly in accordance with the national monitoring regulations  
123 (<http://www.cnemc.cn/jcgf/dqhj/>), and can be acquired from the national urban air quality real-time  
124 publishing platform (<http://106.37.208.233:20035/>). Each monitoring site automatically measures  
125 hourly air pollutants (PM<sub>2.5</sub>, PM<sub>10</sub>, SO<sub>2</sub>, NO<sub>2</sub>, O<sub>3</sub> and CO), and the urban hourly pollutants are  
126 calculated by averaging the pollutants measured at all monitoring sites in that city. The MDA8 O<sub>3</sub>  
127 is calculated based on the hourly O<sub>3</sub> with more than 18-h measurements (Liao et al., 2017). Manual  
128 inspection, including the identification and handling of invalid and lacking data, is performed  
129 following previous studies (Xie et al., 2016; Shu et al., 2017; Zhan et al., 2019).

### 130 **2.2 Surface and sounding meteorological data**

131 With respect to surface observed meteorological data, stations at the three provincial capital  
132 cities (Hefei, Nanjing and Hangzhou) and the megacity Shanghai are selected, which are ZSOF  
133 (117.23°E, 31.87°N), ZSNJ (118.80°E, 32.00°N), ZSHC (120.17°E, 30.23°N), and ZSPD (121.77°E,  
134 31.12°N), respectively. These surface observations, including 2-m temperature, 10-m wind speed  
135 and direction and 2-m relative humidity, are recorded hourly and can be obtained from the website  
136 of the University of Wyoming (<http://weather.uwyo.edu/surface/>). The precipitation data is not  
137 included in the dataset.

138 To verify the upper-air fields, the sounding observations at Shanghai (121.46°E, 31.40°N) and  
139 Nanjing (118.80°E, 32.00°N) are used. These sounding observations (pressure, temperature, relative  
140 humidity, wind direction and wind speed etc.) are also acquired from the website of the University  
141 of Wyoming (<http://weather.uwyo.edu/upperair/sounding.html>), with a time resolution of 12 h

142 (00:00 and 12:00 UTC).

### 143 **2.3 The best-track TC dataset**

144 To capture the characteristics of landfall typhoons, the best-track TC dataset issued by the  
145 China Meteorological Center (CMA) is considered due to its good performance on the landfall  
146 typhoons in the mainland China (available at [http://tcdata.typhoon.org.cn/zjljsjj\\_sm.html](http://tcdata.typhoon.org.cn/zjljsjj_sm.html)). The  
147 dataset covers seasons from 1949 to the present, the region north of the equator and west of 180°E,  
148 and is updated annually (Li and Hong, 2016; Ying et al., 2014). A wealth of information on typhoon  
149 is recorded every 6h in the dataset, including location, minimum sea level pressure, etc. For landfall  
150 typhoons, 24h before their landing and during their activities in the mainland China, the  
151 meteorological data are recorded every 3h. Refer to the national standard for grade of tropical  
152 cyclones (GB/T 19201-2006), the intensity category (IC) of tropical cyclones is provided in the  
153 dataset, which is based on the near surface maximum 2-min mean wind speed near the tropical  
154 cyclone center, ranging from 1 to 6 (Table 1).

155

156 **Table 1. The intensity category of tropical cyclones**

Intensity category (IC)	The near surface maximum 2-min mean wind speed near the tropical cyclone center (m/s)	Beaufort scale
Tropical depression (IC=1)	10.8-17.1	6-7
Tropical storm (IC=2)	17.2-24.4	8-9
Severe tropical storm (IC=3)	24.5-32.6	10-11
Typhoon (IC=4)	32.7-41.4	12-13
Severe typhoon (IC=5)	41.5-50.9	14-15
Super typhoon (IC=6)	≥ 51.0	≥16

157

### 158 **2.4 Model description and configurations**

159 To simulate the high O<sub>3</sub> episodes over the YRD during the typhoon periods, the WRF-CMAQ  
160 one-way coupled model is applied, which consists of WRF v3.6.1  
161 (<https://www2.mmm.ucar.edu/wrf/users/>) developed by the United States National Center for  
162 Atmospheric Research (NCAR) and CMAQ v5.0.2 (<https://github.com/USEPA/CMAQ/tree/5.0.2>)

163 developed by the United States Environmental Protection Agency (EPA).

164 WRF generates offline meteorological inputs for CMAQ with initial and boundary conditions  
165 from the National Centers for Environmental Prediction (NCEP) global final analysis fields every  
166 6 h at a spatial resolution of  $1^\circ \times 1^\circ$  (<https://rda.ucar.edu/datasets/ds083.2/>). Three nested domains  
167 are used, with horizontal resolutions of 81, 27 and 9 km, and grids of  $88 \times 75$ ,  $85 \times 79$  and  $97 \times 97$ ,  
168 respectively (Figure 1a). There are 24 vertical sigma layers from surface to 100 hPa, with about 8  
169 layers located below 1.5 km to resolve the boundary layer processes. Furthermore, the major  
170 physical options for the dynamic parameterization in WRF are summarized in Table 2.

171

172 **Table 2. The domains and physical options for WRF in this study**

Items	Contents
Dimensions (x, y)	(88, 75), (85, 79), (97, 97)
Grid spacing (km)	81, 27, 9
Microphysics	WRF Single-Moment 5-class scheme (Hong et al., 2004)
Longwave radiation	RRTM scheme (Mlawer et al., 1997)
Shortwave radiation	Goddard scheme (Kim and Wang, 2011)
Surface layer	Moni-Obukhov scheme (Monin and Obukhov, 1954)
Land-surface layer	Noah land-surface model (Chen and Dudhia, 2001)
Planetary boundary layer	YSU scheme (Hong et al., 2006)
Cumulus parameterization	Grell-Devenyi ensemble scheme (Grell and Devenyi, 2002)

173

174 Since the horizontal domains of CMAQ are one grid smaller than WRF, all three nested  
175 domains are adjusted automatically. The vertical layers of CMAQ are the same as WRF. The  
176 Meteorology Chemistry Interface Processor (MCIP) can convert WRF outputs to the necessary  
177 meteorological inputs for CMAQ. Moreover, the CB05 gas-phase mechanism with aqueous/cloud  
178 chemistry is selected in the CMAQ configurations.

179 The anthropogenic emissions are from the Multi-resolution Emission Inventory for China  
180 (MEIC) in 2016 with the resolution of  $0.25^\circ$  (<http://meicmodel.org/>), including anthropogenic  
181 emissions from power generation, industry, agriculture, residential and transportation sectors. All

182 emission estimates are spatially allocated to the relevant grid cells based on the meteorological fields  
 183 obtained from WRF, and are temporally distributed on an hourly basis. The simulation starts from  
 184 00:00 UTC on 13 July to 00:00 UTC 27 August, with the first 72 h as spin-up time.

### 185 **2.5 Integrated process rate (IPR) analysis**

186 To quantify the contributions of individual processes to O<sub>3</sub> formation, the IPR analysis  
 187 provided in the CMAQ is utilized. The IPR analysis can illustrate the contributions to changes in  
 188 pollutant concentrations from seven different types of processes, including horizontal advection  
 189 (HADV), vertical advection (ZADV), horizontal diffusion (HDIF), vertical diffusion (VDIF), dry  
 190 deposition (DDEP), cloud processes with the aqueous chemistry (CLDS) and chemical reaction  
 191 process (CHEM), with a mass conservation adjustment at each model grid cell. The IPR analysis  
 192 has been widely applied to investigate regional air pollution (Fan et al., 2015; Li et al., 2012; Wang  
 193 et al., 2010). In this study, MADV is defined as the sum of HADV and ZADV, and TDIF is defined  
 194 as the sum of HDIF and VDIF.

### 195 **2.6 Model evaluation**

196 To evaluate the model performance, the simulation results in the innermost domain, including  
 197 O<sub>3</sub> concentration, air temperature at 2 m (T<sub>2</sub>), relative humidity (RH), wind speed at 10 m (WS<sub>10</sub>)  
 198 and wind direction at 10 m (WD<sub>10</sub>), are examined against the hourly observations at the  
 199 representative cities (Table 3). The statistical metrics, including correlation coefficient (R), root-  
 200 mean-square error (RMSE) and normalized mean bias (NMB), are used. They are defined as follows:

$$201 \quad R = \frac{\sum_{i=1}^N (S_i - \bar{S})(O_i - \bar{O})}{\sqrt{\sum_{i=1}^N (S_i - \bar{S})^2} \sqrt{\sum_{i=1}^N (O_i - \bar{O})^2}}, \quad (3)$$

$$202 \quad RMSE = \sqrt{\frac{\sum_{i=1}^N (S_i - O_i)^2}{N}}, \quad (4)$$

$$203 \quad NMB = \frac{\sum_{i=1}^N (S_i - O_i)}{\sum_{i=1}^N O_i} \times 100\%, \quad (5)$$

204 where S<sub>i</sub> and O<sub>i</sub> are the simulations and observations, respectively. N is the total number of valid

205 data.  $\bar{S}$  and  $\bar{O}$  are the average value of simulations and observations, respectively. In general, the  
206 model results are acceptable if the values of R, RMSE and NMB are close to 1, 0 and 0, respectively  
207 (Li et al., 2017; Shu et al., 2016; Xie et al., 2016).

## 208 **2.7 Estimate of health impacts**

209 Previous studies showed that surface O<sub>3</sub> pollution can induce a series of adverse health  
210 problems from the incidence and mortality of respiratory diseases (Ghude et al., 2016; Jerrett et al.,  
211 2009; Lelieveld et al., 2015). To arouse more attention on the issue that O<sub>3</sub> can be significantly  
212 affected by typhoons in the YRD, we further estimate the premature mortality attributed to O<sub>3</sub> during  
213 the study period.

214 A standard damage function (Anenverg et al., 2010; Liu et al., 2018; Voorhees et al., 2014;  
215 WS/T 666-2019, Technical specifications for health risk assessment of ambient air pollution of  
216 China) is employed to quantify premature mortality due to O<sub>3</sub> exposure:

$$217 \Delta M = y_0 \left( \frac{RR - 1}{RR} \right) Pop, \quad (1)$$

218 where  $\Delta M$  is the excess mortalities attribute to O<sub>3</sub> exposure,  $y_0$  is the baseline mortality rate, RR is  
219 relative risk and  $(RR-1)/RR$  is the attributable fraction, and Pop is the exposed population. RR can  
220 be calculated using the following relationship:

$$221 RR = \exp(\beta(C - C_0)), \quad (2)$$

222 where  $\beta$  is the concentration-response factor, C is the exposure concentration and  $C_0$  represents the  
223 theoretical minimum-risk concentration.

224 In this study, the mortality rate for respiratory disease is obtained from China Health and  
225 Family Planning Statistical Yearbook 2018 ([https://www.yearbookchina.com/navibooklist-  
226 n3018112802-1.html](https://www.yearbookchina.com/navibooklist-n3018112802-1.html)), which is 68.02/100000. The  $\beta$  is generated from Dong et al. (2016), that is  
227 0.461%. The population data are obtained from the Bureau of Statistics of different cities in the  
228 YRD. The  $C_0$  is 70  $\mu\text{g m}^{-3}$  for MDA8 O<sub>3</sub> given by the World Health Organization (WHO).

229

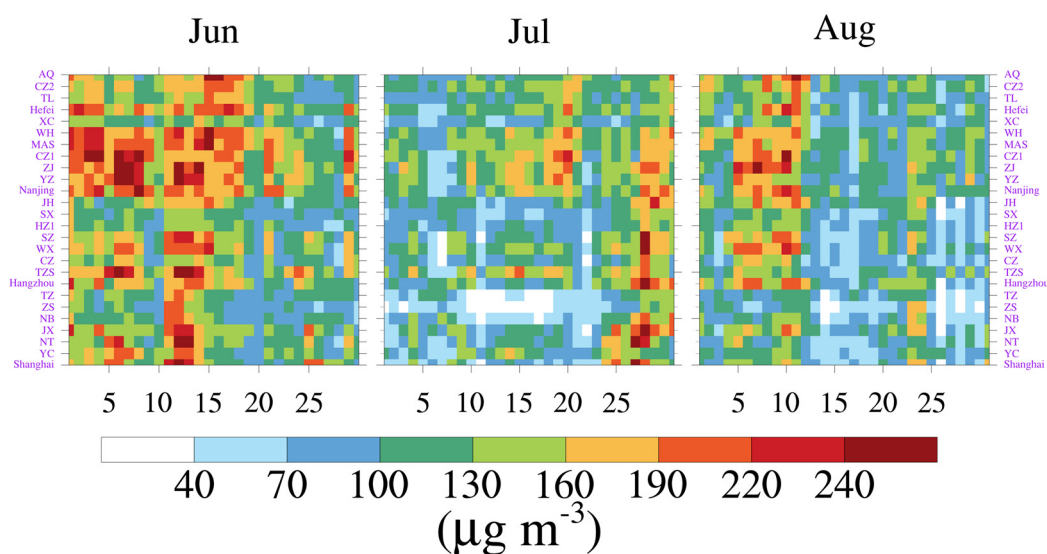
## 230 **3 Results and discussions**

### 231 **3.1 Characteristic of O<sub>3</sub> episodes**

232 In the midsummer, the warm sea surface (high temperature) is conducive to the generation of  
233 typhoons (high O<sub>3</sub> concentration), providing a good opportunity to investigate the mechanism of

234 typhoons affecting O<sub>3</sub> in the YRD. Figure 2 shows the MDA8 O<sub>3</sub> in the typical 26 cities of the YRD  
 235 in summer of 2018. Actually, it is common for typhoons to affect O<sub>3</sub> in the YRD during summer,  
 236 and 2018 is special because there were 8 landfall typhoons and many of them landed further north  
 237 than in the normal years (see Supplement for details). O<sub>3</sub> concentration was relatively high in June,  
 238 and relatively low in July and August. The relatively low O<sub>3</sub> may be attributed to the maritime air  
 239 masses transported by the Asian summer monsoon (Ding et al., 2008; Xu et al., 2008). Nevertheless,  
 240 we notice that there are two regional multiday O<sub>3</sub> pollution episodes from 24 July to 11 August in  
 241 the YRD, which means that about half of the cities in the YRD exceed the national air quality  
 242 standard (The national ambient air quality standard for MDA8 O<sub>3</sub> is 160 μg m<sup>-3</sup> in China). The first  
 243 multiday O<sub>3</sub> episodes appeared in most of the cities from 24 July to 2 August. The highest MDA8  
 244 O<sub>3</sub> concentration reached up to 264 μg m<sup>-3</sup> on 27 July in Ningbo (NB). O<sub>3</sub> pollution was even  
 245 observed for 6 consecutive days from 27 July to 1 August in Maanshan (MAS). Only two days later,  
 246 regional O<sub>3</sub> pollution occurred in the YRD again from 5 August to 11 August.

247

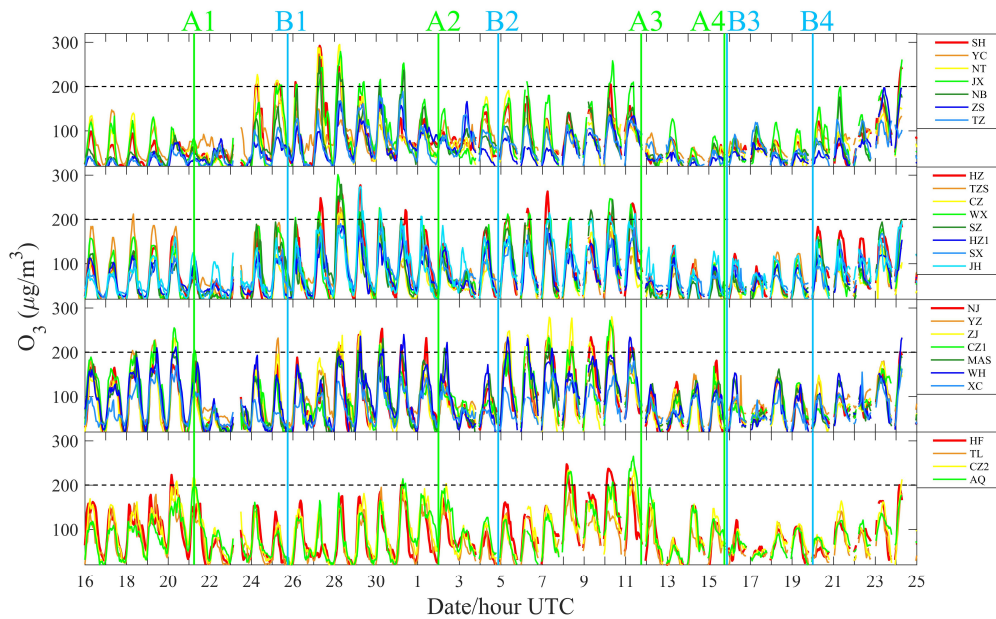


248  
 249 **Figure 2. The MDA8 O<sub>3</sub> in 26 cities of the YRD in June (left panel), July (middle panel), and**  
 250 **August (right panel) 2018. The national ambient air quality standard for MDA8 O<sub>3</sub> is 160 μg**  
 251 **m<sup>-3</sup> in China. These cities are sorted by longitude.**

252  
 253 Figure 3 further shows diurnal variation of O<sub>3</sub> in all 26 cities of the YRD from 00:00 16 July  
 254 to 00:00 25 August (throughout this paper the time refers to UTC, unless LST is specifically stated).



255 Interestingly, O<sub>3</sub> pollution occurred earlier in cities near the coastline (e.g. large longitudes in °E,  
 256 Figure 1b) rather than concurrently during the two multiday O<sub>3</sub> episodes. For example, from 24 July  
 257 to 2 August, the first day that hourly O<sub>3</sub> concentration exceeded the national air quality standard  
 258 (The national ambient air quality standard for hourly O<sub>3</sub> is 200 µg m<sup>-3</sup> in China) in Shanghai,  
 259 Hangzhou, Nanjing and Hefei was 24 July, 27 July, 28 July and 31 July, respectively. Thus, we  
 260 classify the 26 cities in the YRD into four categories based on their longitudes, surrounding the four  
 261 representative cities (Figure 4). The category I cities include SH, YC, NT, JX, NB, ZS and TZ. The  
 262 category II cities include HZ, TZS, CZ, WX, SZ, HZ1, SX and JH, and the category III cities include  
 263 NJ, YZ, ZJ, CZ1, MAS, WH and XC. Other cities are classified as the category IV cities, which are  
 264 HF, TL, CZ2 and AQ. The first category cities are closest to the coastline, while the fourth category  
 265 is the opposite.  
 266



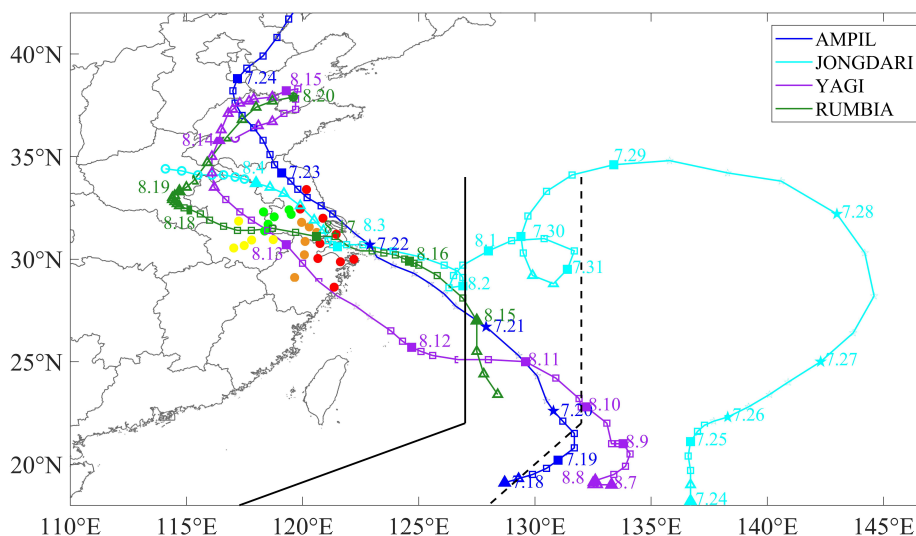
267  
 268 **Figure 3. Diurnal variation of O<sub>3</sub> in 26 cities of the YRD from 16 June to 25 August, 2018. The**  
 269 **grey dotted lines are the national ambient air quality standard for hourly O<sub>3</sub> (200 µg m<sup>-3</sup>) in**  
 270 **China. The letter A indicates the moment that the typhoon has reached the 24-h warning line,**  
 271 **and letter B indicates the last moment when the typhoon was active in the mainland China.**  
 272 **These times are acquired from the best-track TC dataset, depending on the start and end times**  
 273 **of the 3h observations. Coordinates 1, 2, 3, and 4 represent Typhoon Ampil, Typhoon Jongdari,**  
 274 **Typhoon Yagi, and Typhoon Rumbia, respectively. Note: these cities are sorted by longitude.**

275

### 276 3.2 Landfall typhoons and their effects

277 O<sub>3</sub> episodes with regional and long-lasting characteristics may often be associated with slow-  
278 moving synoptic weather systems. We find that the O<sub>3</sub> episodes coincided well with activities of  
279 landfall typhoons, showing in their tracks and intensities in Figure 4. Typhoon Ampil was first  
280 observed at 00:00 on 18 July, and landed in Shanghai around 4:30 on 22 July with an intensity of  
281 severe tropical storm (IC=3). While Typhoon Ampil remained active, Typhoon Jongdari generated  
282 over the western North Pacific at 12:00 on 23 July, and made landfall at the junction of Zhejiang  
283 province and Shanghai at 21:00 1 August. After Typhoon Jongdari, Typhoon Yagi generated at 00:00  
284 7 August. At around 15:35 12 August, it landed in Zhejiang province and remained active in the  
285 mainland China until 21:00 15 August. Before the end of Typhoon Yagi, Typhoon Rumbia was  
286 observed over the western North Pacific at 6:00 14 August. It finally landed in Shanghai at around  
287 20:00 16 August, causing huge economic losses.

288



289

290 **Figure 4. The track and intensity of Typhoon Ampil, Typhoon Jongdari, Typhoon Yagi, and**  
291 **Typhoon Rumbia. The track is labeled with the date of the month and day (in month.day).**  
292 **The circle, triangle, square and pentagram indicate the intensity category of tropical cyclones**  
293 **is less than 1 (IC < 1), equal to 1 (IC = 1), equal to 2 (IC = 2), and not less than 3 (IC >= 3),**  
294 **respectively. Black solid line and dotted line represent the 24-hour and 48-h warning line for**  
295 **tropical cyclones, respectively. The colored solid points are the locations of cities in the YRD,**

296 **and different color represents different cities categories. Wherein, red, carrot, green and**  
297 **yellow are category I, II, III and IV cities, respectively.**

298

299 To further understand the relationship between O<sub>3</sub> episodes and landfall typhoons, we mark the  
300 critical moments of landfall typhoons in Figure 3. The letter A indicates the moment when a typhoon  
301 has reached the 24-h warning line, and the letter B indicates the last moment of that typhoon remains  
302 active in the mainland China. These moments are acquired from the best-track TC dataset,  
303 depending on the start and the end time of the 3h observations. Coordinates 1, 2, 3, and 4 represent  
304 Typhoon Ampil, Typhoon Jongdari, Typhoon Yagi, and Typhoon Rumbia, respectively. As shown  
305 in Figure 3, O<sub>3</sub> exhibited a significant cycle during the study period. That is, when the typhoon is  
306 close enough (near moments A1, A2, A3 and A4), the O<sub>3</sub> concentrations decreased, but O<sub>3</sub>  
307 concentrations would increase as long as the typhoon was not active in the mainland China (B1, B2  
308 and B4) any more. This cycle would repeat if the next typhoon approached. O<sub>3</sub> pollution was likely  
309 to occur during the period from the end of a typhoon to the arrival of the next typhoon (B1A2 and  
310 B2A3) in the YRD.

311 Furthermore, we find that the variations of O<sub>3</sub> was related to the track, duration and landing  
312 intensity of the typhoons. For example, during the B1A2 period when the O<sub>3</sub> pollution occurred, the  
313 moments that hourly O<sub>3</sub> concentrations first exceed 200 µg m<sup>-3</sup> in about half of cities of the  
314 categories I, II, III and IV were 6:00 UTC (14:00 LST) 27 July, 6:00 UTC (14:00 LST) 28 July, 3:00  
315 UTC (11:00 LST) 29 July and 6:00 UTC (14:00 LST) 31 July, respectively. This phenomenon also  
316 suggests that O<sub>3</sub> pollution first occurs in cities along the coastline, which may be related to the track  
317 of typhoons (Figure 4). Regarding the impact of typhoon duration, the A4B3 period provided a good  
318 interpretation. While Typhoon Yagi was still active in the mainland China, Typhoon Rumbia had  
319 reached the 24-hour warning line. Hence, the O<sub>3</sub> remained a low level throughout the period (A3B4),  
320 which was quite different from B1A2 and B2A3 period. Noted that the landing point and active path  
321 of Typhoon Ampil and Typhoon Jongdari were very similar (Figure 4). However, the landing  
322 intensity of Typhoon Ampil was severe tropical storm (IC = 3), and that of Typhoon Jongdari was  
323 tropical storm (IC = 2), resulting in a difference in O<sub>3</sub> concentrations for Shanghai. Within 24 hours  
324 after Typhoon Ampil (Jongdari) reached the 24-hour warning line, the average O<sub>3</sub> concentrations  
325 reached 40.9 (80.1) µg m<sup>-3</sup> in Shanghai. This is because that the stronger the typhoon landed, the

326 gale (The 10-m wind speed near moment A1 was larger than that near moment A2 in Shanghai,  
327 Figure 7a) and precipitation accompanying the typhoon will be more effective in removing O<sub>3</sub>.

### 328 **3.3 Processes of O<sub>3</sub> pollution affecting by typhoons**

329 To reveal the major processes of O<sub>3</sub> pollution episodes affected by landfall typhoons, one  
330 municipality and three provincial capital cities with different longitudes, including Shanghai  
331 (121.77°E, 31.12°N), Hangzhou (120.17°E, 30.23°N), Nanjing (118.80°E, 32.00°N) and Hefei  
332 (117.23°E, 31.87°N), are selected for further analysis – based on monitoring data and model results.

#### 333 **3.3.1 Evaluation of model performance**

334 To evaluate the simulation performance, the hourly simulation results are compared with the  
335 measurements from 00:00 16 July to 00:00 25 August. Table 3 presents the statistical metrics for  
336 selected variables, including temperature at 2 m (T<sub>2</sub>), relative humidity (RH), wind speed at 10 m  
337 (WS<sub>10</sub>), wind direction at 10 m (WD<sub>10</sub>), and surface O<sub>3</sub>. T<sub>2</sub> is reasonably well simulated, with R  
338 values of 0.75, 0.77, 0.72 and 0.64 in Shanghai, Hangzhou, Nanjing and Hefei, respectively. Though  
339 our simulation underestimates T<sub>2</sub> to some extent, this slight underestimation is acceptable because  
340 of the small RMSE (3.2, 2.7, 2.9 and 3.3) and NMB (-7.5%, -5.1%, -5.5% and -5.5%) values. As  
341 for RH, the simulation results are overestimated in all four cities, leading to the NMB values of  
342 9.1%, 4.6%, 6.7% and 0.5% in Shanghai, Hangzhou, Nanjing and Hefei, respectively. With high R  
343 values (0.69, 0.65, 0.71 and 0.71) and relatively low RMSE values (12.4, 12.8, 12.1 and 10.8), the  
344 WRF simulates RH over the YRD quite well. The wind fields are closely related to the transport  
345 processes of air pollutants. The overestimation of WS<sub>10</sub> may partly be attributed to the unresolved  
346 terrain features by the default surface drag parameterization causing overestimation of wind speed  
347 in particular at low values (Jimenez and Dudhia, 2012; Li et al., 2017). With regards to WD<sub>10</sub>, the  
348 simulation error is large based only on these statistical metrics. This is because that near-surface  
349 wind fields are deeply influenced by local underlying surface characteristics, and improving the  
350 urban canopy parameters might be useful (Liao et al., 2015; Xie et al., 2016). In term of O<sub>3</sub>, the  
351 simulated O<sub>3</sub> concentrations behave satisfactorily. R is 0.55, 0.65, 0.66 and 0.54 for the simulations  
352 for Shanghai, Hangzhou, Nanjing and Hefei, respectively, while the NMB values are 5.8%, 16.4%,  
353 -6.2% and -5.3%, respectively.

354

355 **Table 3. Statistical metrics in meteorological variables and O<sub>3</sub> concentration between the**

**observations and simulations.**

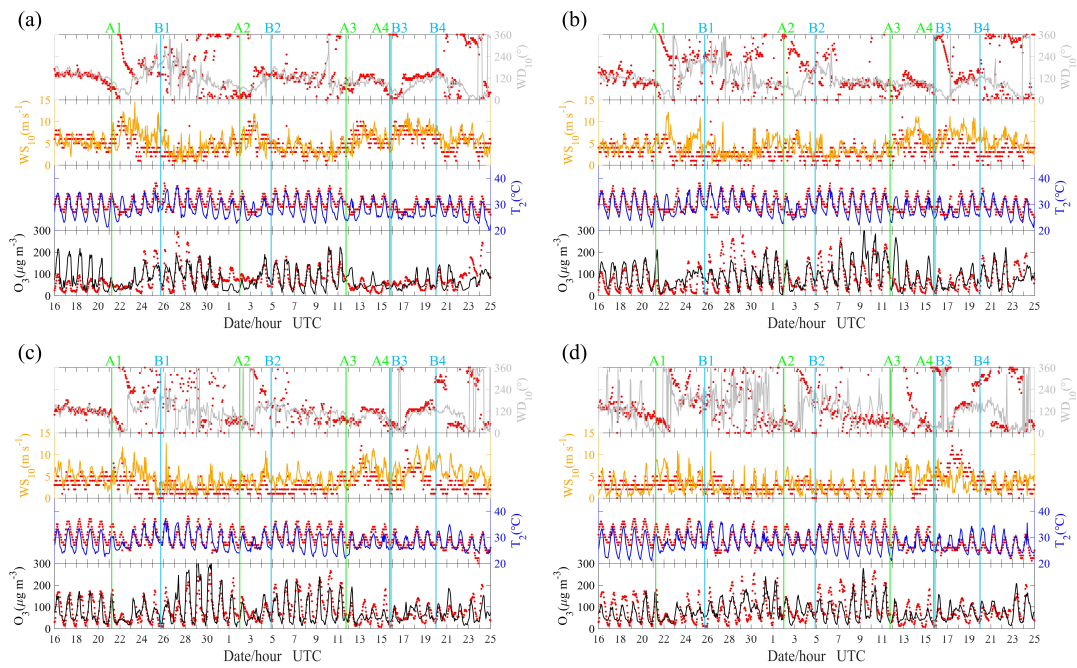
City	Variable	$\bar{O}$	$\bar{S}$	R	RMSE	NMB
Shanghai	T <sub>2</sub> (°C)	30.3	28.1	0.75	3.2	-7.5%
	RH (%)	75.0	81.8	0.69	12.4	9.1%
	WS <sub>10</sub> (m s <sup>-1</sup> )	4.9	5.5	0.51	2.3	11.7%
	WD <sub>10</sub> (°)	144.8	113.4	0.01	113.5	-22.9%
	O <sub>3</sub> (μg m <sup>-3</sup> )	74.3	76.5	0.55	45.3	5.8%
Hangzhou	T <sub>2</sub> (°C)	30.3	28.8	0.77	2.7	-5.1%
	RH (%)	75.1	78.5	0.65	12.8	4.6%
	WS <sub>10</sub> (m s <sup>-1</sup> )	3.3	4.7	0.32	2.7	32.5%
	WD <sub>10</sub> (°)	155.0	114.7	-0.10	132.5	-27.8%
	O <sub>3</sub> (μg m <sup>-3</sup> )	81.7	91.3	0.65	49.8	16.4%
Nanjing	T <sub>2</sub> (°C)	29.8	28.1	0.72	2.9	-5.5%
	RH (%)	77.4	82.6	0.71	12.1	6.7%
	WS <sub>10</sub> (m s <sup>-1</sup> )	3.1	5.0	0.39	3.0	63.8%
	WD <sub>10</sub> (°)	132.8	115.6	0.21	102.7	-15.0%
	O <sub>3</sub> (μg m <sup>-3</sup> )	87.6	79.8	0.66	46.7	-6.2%
Hefei	T <sub>2</sub> (°C)	29.3	27.7	0.64	3.3	-5.5%
	RH (%)	81.1	81.5	0.71	10.8	0.5%
	WS <sub>10</sub> (m s <sup>-1</sup> )	3.2	3.2	0.37	2.2	2.9%
	WD <sub>10</sub> (°)	147.0	128.6	0.04	136.7	-13.3%
	O <sub>3</sub> (μg m <sup>-3</sup> )	87.3	80.3	0.54	45.0	-5.3%

357 *Note.* R exceeds 0.1 to reach statistically significant at 99.9% confident level.  $\bar{O}$  and  $\bar{S}$  are the  
358 average values of the observations and simulations, respectively.

359

360 Figure 5 further shows hourly variations of O<sub>3</sub>, T<sub>2</sub>, WS<sub>10</sub> and WD<sub>10</sub> for measurements and  
361 simulations in four representative cities. The simulations effectively reproduce the diurnal variation  
362 of O<sub>3</sub>, T<sub>2</sub> and WS<sub>10</sub>, confirming the reliability of the simulation results. Moreover, the model well  
363 captures the shift in wind direction during the study period. Thus, the overall model performance in  
364 simulating wind fields is acceptable. In summary, the simulations can capture and reproduce the  
365 major meteorological characteristics and O<sub>3</sub> evolution during the O<sub>3</sub> episodes, and thus can provide  
366 valuable insights into the formation of the O<sub>3</sub> episodes.

367



368

369

370 **Figure 5. Hourly variations of  $O_3$ ,  $T_2$ ,  $WS_{10}$  and  $WD_{10}$  in measurements (red dots) and**  
 371 **simulation (colored lines) in (a) Shanghai, (b) Hangzhou, (c) Nanjing and (d) Hefei.**

372

### 373 3.3.2 Shanghai in category I cities

374 In the study period, Shanghai was usually one of the first cities affected by landfall typhoons.

375 We can see a multiday episode of  $O_3$  during the period of 24-28 July, with a maximum of hourly  $O_3$

376 up to  $292 \mu\text{g m}^{-3}$  at 27 July (Figure 6a). The high  $O_3$  concentrations together with high primary

377 pollutants ( $\text{CO}$  and  $\text{NO}_2$ ) suggest a strong photochemical  $O_3$  production under the condition of high

378 temperature (The daily maximum temperature can reach  $35 \text{ }^\circ\text{C}$ ) during this period, and the weak

379 wind may play a significant role in the accumulation of surface  $O_3$ . The increase of the primary

380 pollutants may be related to a change in wind direction from southeast to southwest causing by

381 Typhoon Ampil (A1 in Figure 6a, -A1 and A1B1 in Figure 7), which originally brought air mass

382 from the ocean, shifted to from inland. Interestingly,  $\text{PM}_{2.5}$  also showed good correlation with  $O_3$

383 and primary pollutants, especially for  $\text{NO}_2$  during this period. This indicates that a high level of

384 oxidizability can promote the formation of secondary particles (Kamens et al., 1999; Khoder, 2002).

385 From the results of process analysis (Figure 6b), the major contributions to surface  $O_3$  were TDIF,

386 CHEM and DDEP due to the small net contribution of MADV. TDIF had a considerable positive

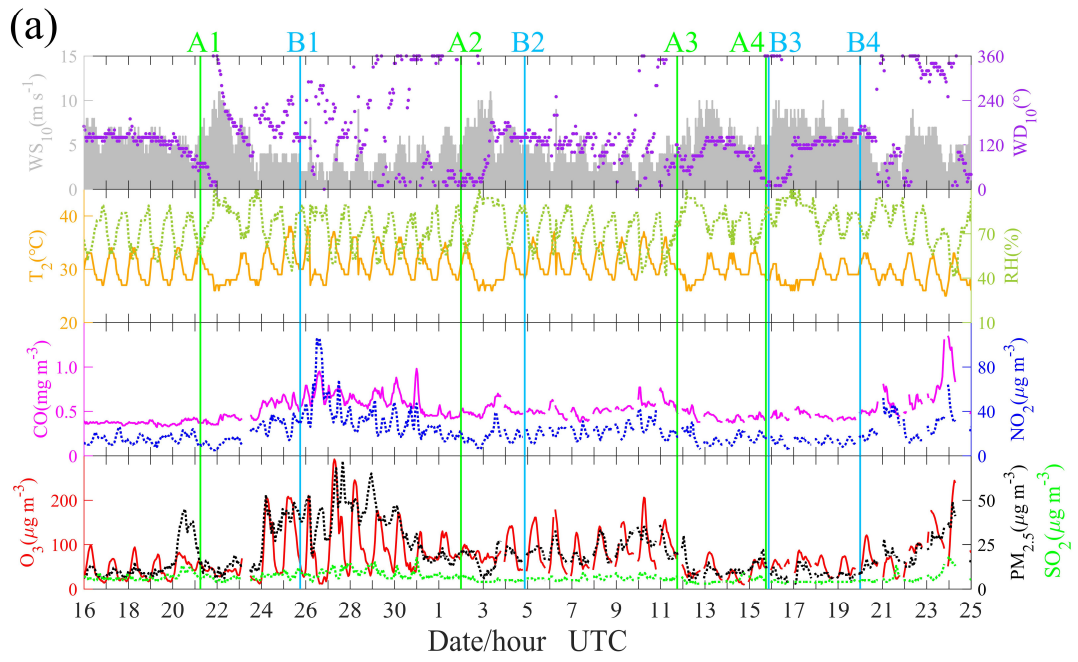
387 contribution while DDEP did the opposite, suggesting that high surface  $O_3$  may be sourced from the

388 upper layer via TDIF process, and be removed via DDEP process. However, for the whole boundary

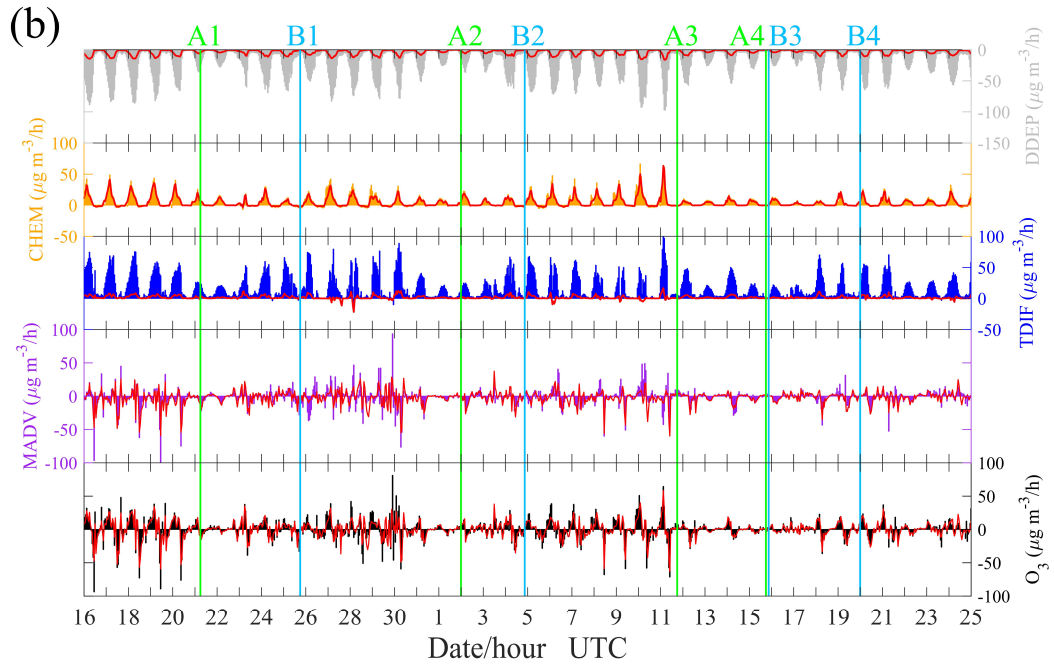
389 layer, which is defined as the layer less than 1500 m in this study, the balance was between CHEM  
390 and DDEP instead TDIF and DDEP. Thus, TDIF was likely to play the role of “transport” from the  
391 upper layer to surface. Figure 6c further shows the temporal-vertical distribution of O<sub>3</sub> with vertical  
392 wind velocity. The downward airflows prevailed over Shanghai until 23 July, which are induced by  
393 the subtropical high. Then, strong upward airflows appeared as Typhoon Ampil arrived, and high  
394 level of O<sub>3</sub> disappeared. Around 27 July, the downward airflows gradually resumed and high level  
395 of O<sub>3</sub> occurred. The downward airflows are critical because they can not only inhibit the vertical  
396 transport of O<sub>3</sub> but also transport high-level O<sub>3</sub> to the surface. The high-level O<sub>3</sub> in the troposphere  
397 mainly comes from two sources. One is that O<sub>3</sub>-rich air from the low stratosphere transported by  
398 the downdrafts in large-scale typhoon circulation (Jiang et al., 2015). The other is that O<sub>3</sub> produced  
399 by photochemical reactions during the day. It is noteworthy that high photochemical production  
400 efficiency of O<sub>3</sub> occurred in the middle boundary layer instead of at the surface. Moreover, most of  
401 the O<sub>3</sub> remained in the residual layer at night, while surface O<sub>3</sub> concentration was much lower due  
402 to NO<sub>x</sub> titration. By the second day, high O<sub>3</sub> in the residual layer was transported to the surface by  
403 the downward airflows as air in the boundary layer is gradually mixed. Combined with the newly  
404 generated O<sub>3</sub>, a high concentration of O<sub>3</sub> would eventually appear on the surface.

405 As shown in Figure 7, O<sub>3</sub> pollution tends to occur during the period from the end of a typhoon  
406 to the arrival of the next typhoon (B1A2 and B2A3) in the YRD. To reveal this phenomenon, we  
407 compare these two periods (B1A2 and B2A3) with their previous periods (A1B1 and A2B2) using  
408 the skew-T log-P diagram (Figure 6d and 6e). It is found that the atmospheric conditions of B1A2  
409 (B2A3) were hotter and drier than A1B1 (A2B2) below 700 hPa in Shanghai, and wind speed is  
410 smaller in B1A2 (B2A3). Those changes in atmospheric conditions after typhoon will be conducive  
411 to the generation of high O<sub>3</sub> concentration in Shanghai.

412

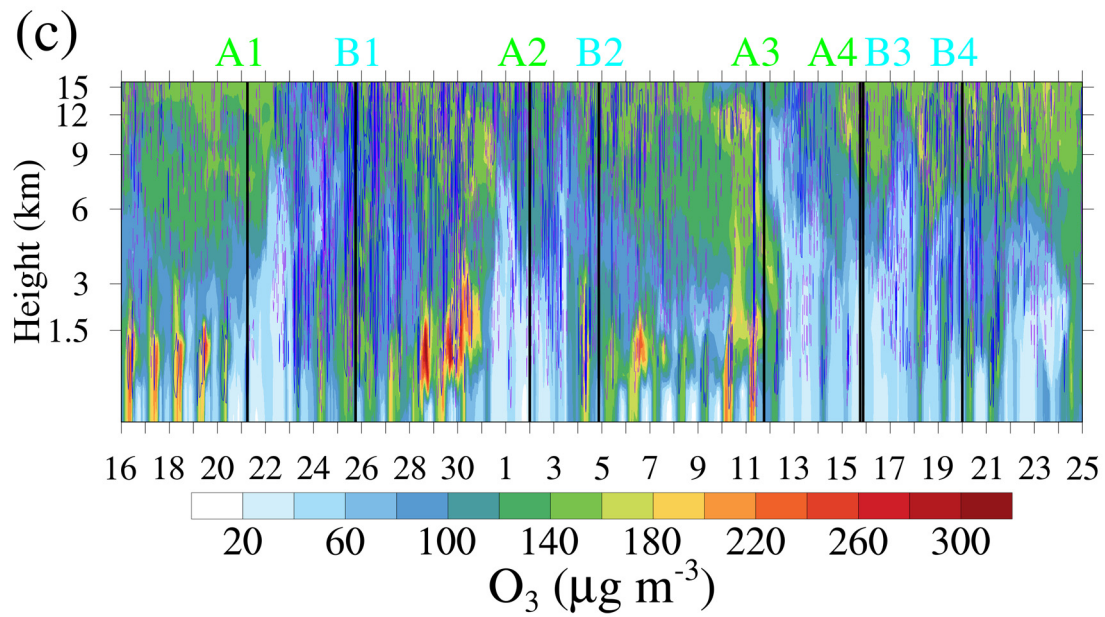


413

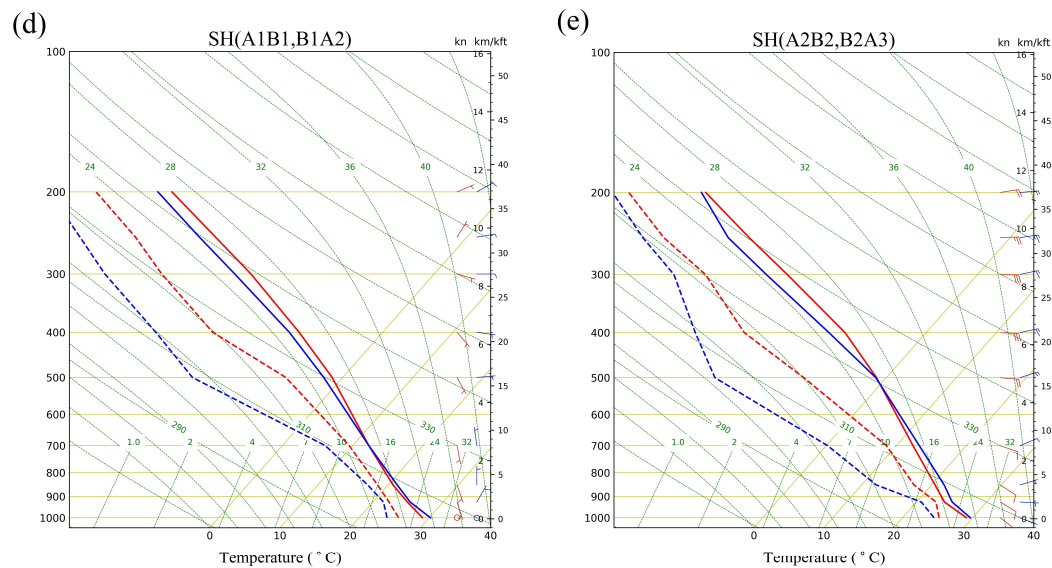


414





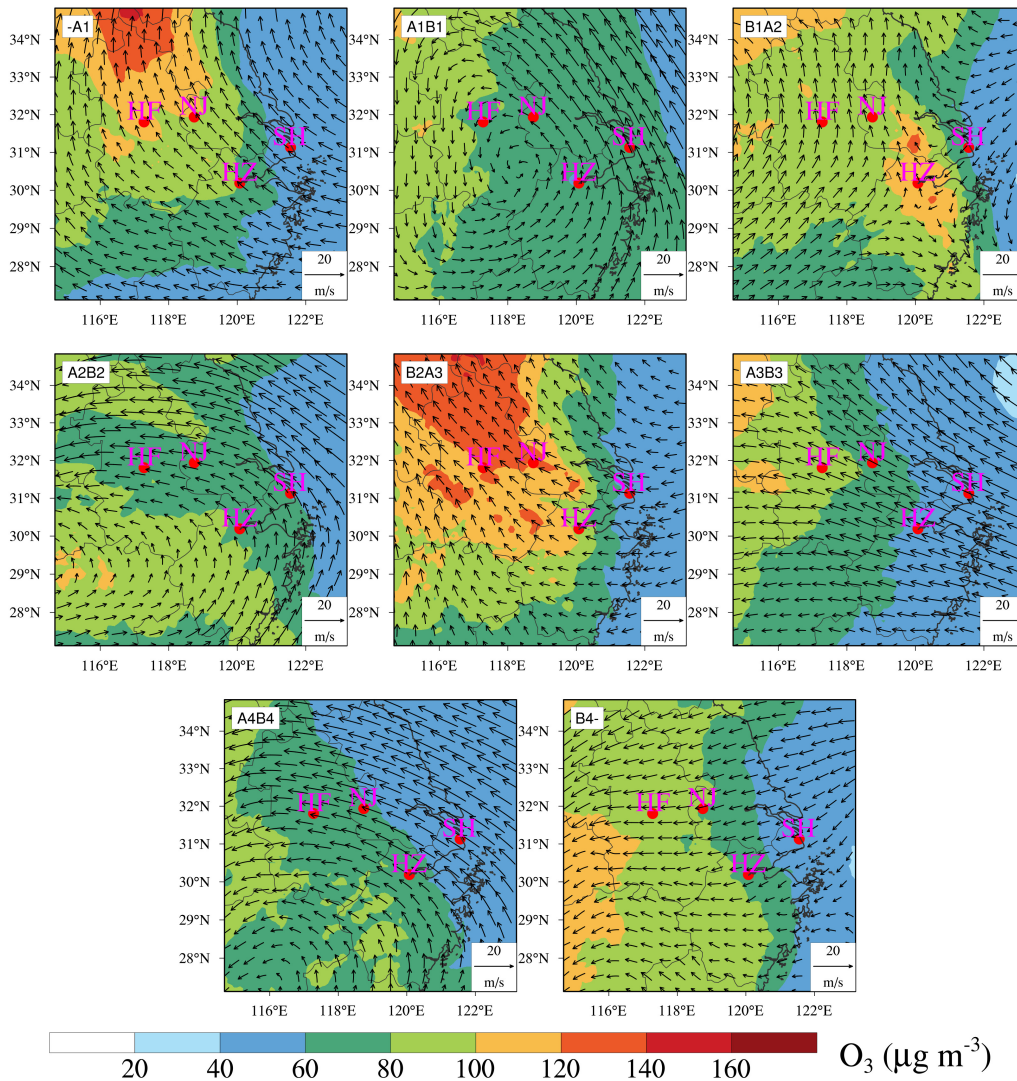
415



416

417 **Figure 6. (a) Time series of air pollutants ( $O_3$ ,  $PM_{2.5}$ ,  $SO_2$ ,  $CO$  and  $NO_2$ ) and meteorological**  
 418 **factors ( $T_2$ ,  $RH$ ,  $WS_{10}$  and  $WD_{10}$ ) in Shanghai. (b) Individual processes contribution to net  $O_3$**   
 419 **density at Shanghai.  $O_3$  is the net increase, MADV is the sum of horizontal advection (HADV)**  
 420 **and vertical advection (ZADV), TDIF is the sum of horizontal diffusion (HDIF) and vertical**  
 421 **diffusion (VDIF), CHEM is the chemical reaction process, and DDEP is the dry deposition**  
 422 **process. The color histograms indicate the results for the layer near the surface, while the solid**  
 423 **red lines indicate the average results for all layers below 1500 m. (c) Temporal-vertical**  
 424 **distribution of  $O_3$  with vertical wind velocity over Shanghai. The dotted purple line and solid**  
 425 **blue line indicate the negative wind speeds (downward airflows) and positive wind speeds**

426 (upward airflows), respectively. (d) The skew-T log-P diagram at Shanghai. The average  
 427 results of period A1B1 and B1A2 are shown in red and blue, respectively. (e) Same as (d), but  
 428 for the average results of period A2B2 and B2A3.  
 429



430  
 431 **Figure 7. Spatial distribution of surface O<sub>3</sub> overlaid with wind fields at 850 hPa over the YRD.**  
 432 **-A1, A1B1, B1A2, A2B2, B2A3, A3B3, A4B4, B4-** are the average results from the beginning  
 433 **to A1, A1 to B1, B1 to A2, A2 to B2, B2 to A3, A3 to B3, A4 to B4, and B4 to the end, respectively.**  
 434 **Details can be found in Figure 4.**

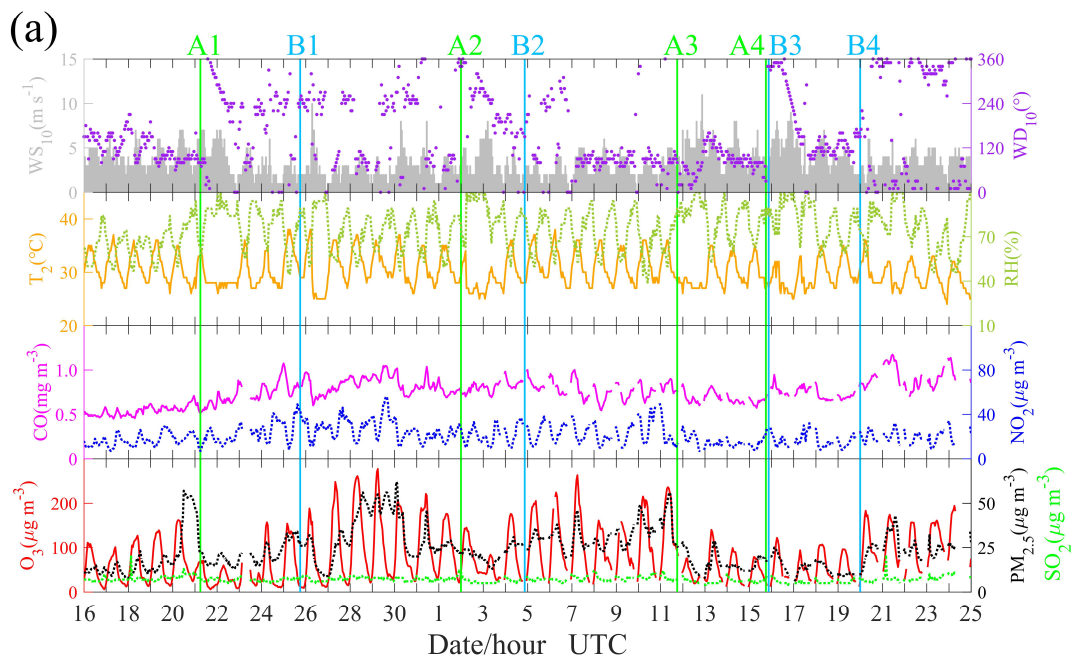
435

### 436 3.3.3 Hangzhou in category II cities

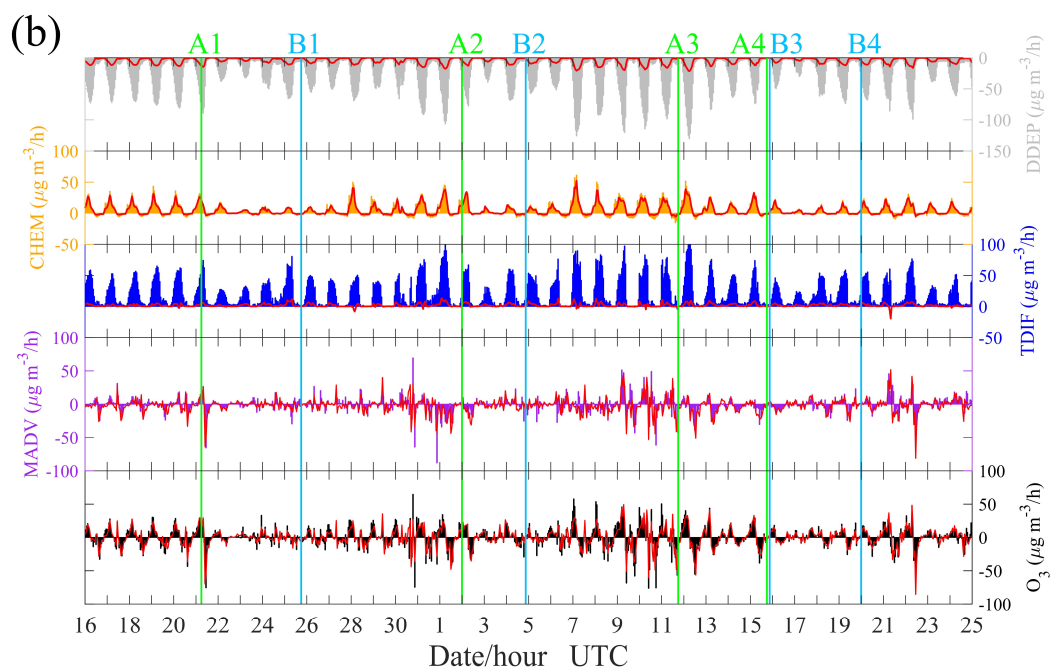
437 Figure 8 presents the case in Hangzhou. It shows that high O<sub>3</sub> concentrations occurred on 27-  
 438 31 July and 5-7 August, which may also be related to the strong photochemical production of O<sub>3</sub>

439 under the abundance of precursors (Figure 8a) and poor diffusion conditions due to the light wind  
 440 (B1A2 and B2A3 in Figure 7). Figure 8a further shows that high O<sub>3</sub> was often associated with an  
 441 increase in CO but the NO<sub>2</sub> concentrations usually remained at the same level. This phenomenon  
 442 indicates a VOCs-limited regime in this city since CO usually have good correlation with VOCs  
 443 and can play a similar role as VOCs in the photochemical production of O<sub>3</sub> (Atkinson, 2000; Ding  
 444 et al., 2013). In fact, O<sub>3</sub> in other representative cities (Shanghai, Nanjing and Hefei) also showed a  
 445 better correlation with CO than NO<sub>2</sub>. Though Hangzhou is close to Shanghai, there is a significant  
 446 difference of wind fields over these two cities. Starting from the arrival of Typhoon Ampil (A1).  
 447 The wind direction in Hangzhou did not change back to southeast until a few days later after  
 448 Typhoon Jongdari dissipated (B2). During this period (A1B2), the frequent southwest wind may be  
 449 the reason for high CO concentrations in Hangzhou. In addition, the chaotic wind field during period  
 450 B1A2 (B1A2 in Figure 7) may lead to the light wind in Hangzhou. With respect to the simulation  
 451 results, the model simulated the variation of O<sub>3</sub> but failed to capture the O<sub>3</sub> peaks (e.g., the peak  
 452 values on 27-31 July), which may be related to the strong upward airflows (Figure 8c) that inhibited  
 453 the accumulation of O<sub>3</sub> (Figure 8b). This further illustrates that downward airflows may be an  
 454 important factor for O<sub>3</sub> episodes in this case.

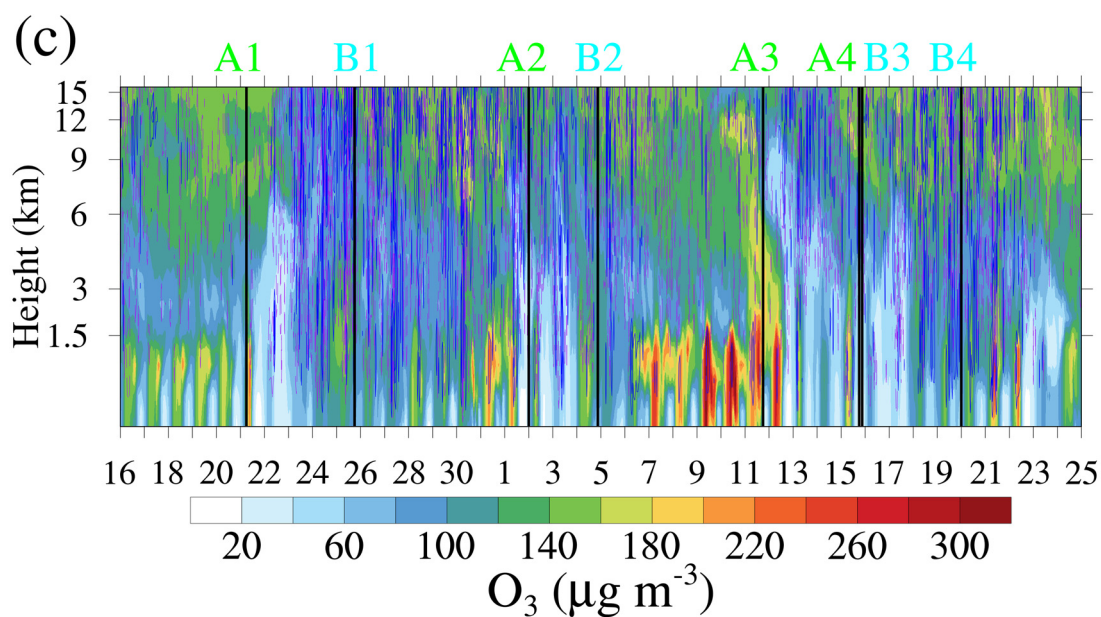
455



456



457



458

459 **Figure 8. Same as Figure 6 (a)-(c), but for Hangzhou.**

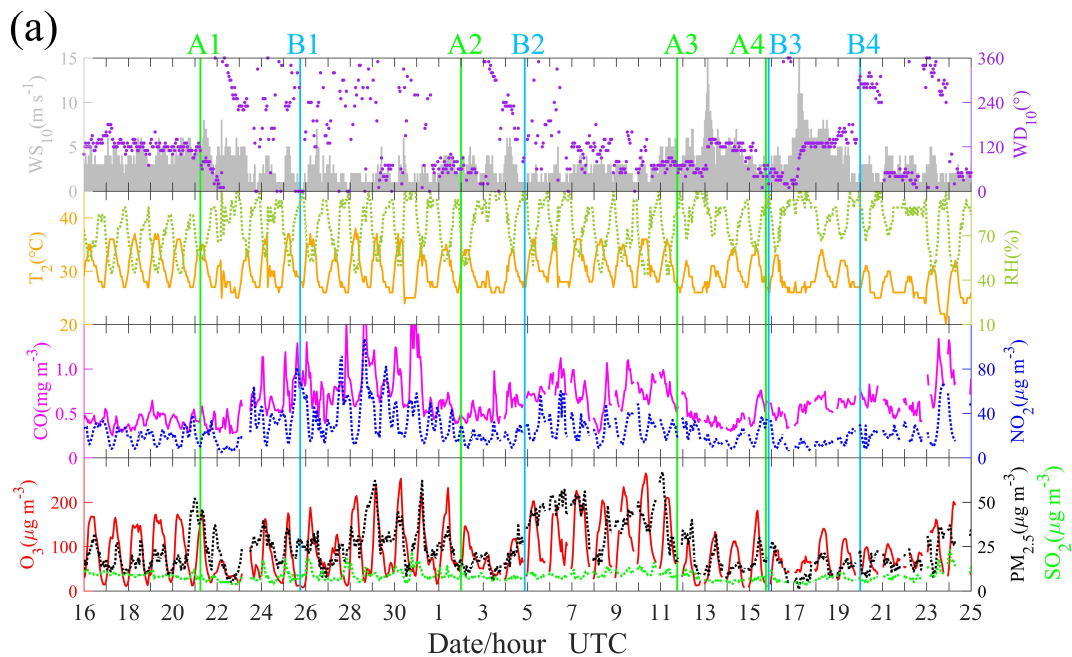
460

### 461 3.3.4 Nanjing in category III cities

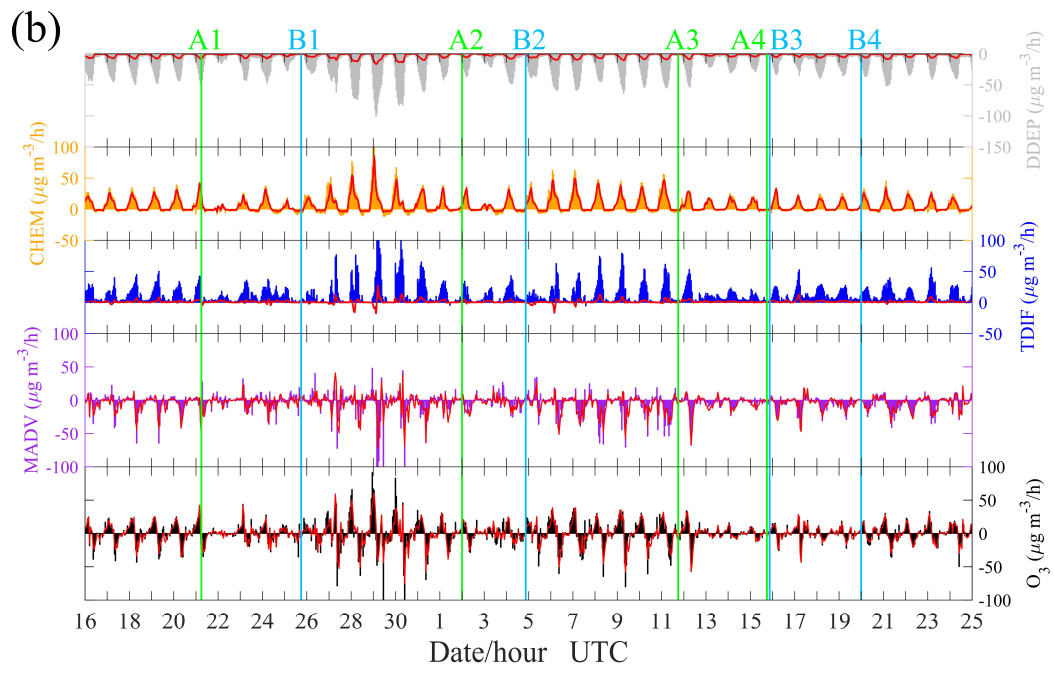
462 In Nanjing, the O<sub>3</sub> episode exceeded the national air quality standards was observed on 28 July  
 463 to 1 August and 7-11 August. These O<sub>3</sub> episodes were characterized by abundant O<sub>3</sub> precursors  
 464 under the condition of high temperature. Furthermore, light wind (B1A2 and B2A3 in Figure 7) and  
 465 downward airflows (Figure 9c) also contributed greatly to the occurrence of O<sub>3</sub> pollution, resulting  
 466 from a mechanism similar to that for Shanghai and Hangzhou. As early as on 22 July, the wind



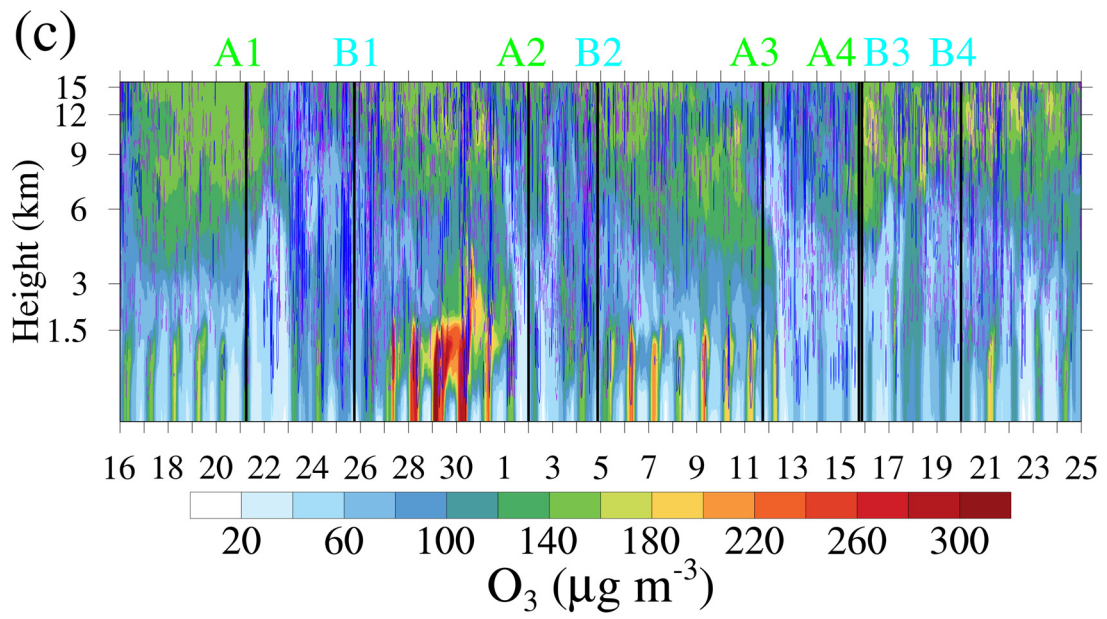
467 direction in Nanjing changed from southeast to southwest because of the arrival of Typhoon Ampil,  
 468 and thus the concentrations of the main primary pollutants (CO, NO<sub>2</sub> and SO<sub>2</sub>) increased (Figure  
 469 9a). However, high-level O<sub>3</sub> episodes did not occur until 28 July even though the maximum  
 470 temperature did not change significantly during 24-31 July. The “obstacle” for enhancing O<sub>3</sub> levels  
 471 may be the precipitation caused by the strong upward airflows during 23-26 July (Figure 9c). As  
 472 shown in Figure 9b, high surface O<sub>3</sub> concentration during the pollution episodes is the result of  
 473 TDIF and CHEM processes, and is lost through DDEP and MADV processes. Regarding vertical  
 474 structure of atmospheric, B1A2 (B2A3) was also hotter and drier than A1B1 (A2B2) below 700 hPa  
 475 in Nanjing (Figure 9d and 9e). These consequences, similar to those in Shanghai, further confirm  
 476 that high O<sub>3</sub> concentrations in a region are more likely to occur during the period from the end of  
 477 an exciting typhoon to the arrival of the next typhoon (B1A2 and B2A3) than during the period  
 478 when a typhoon approaches and is active in the region (A1B1 and A2B2).  
 479



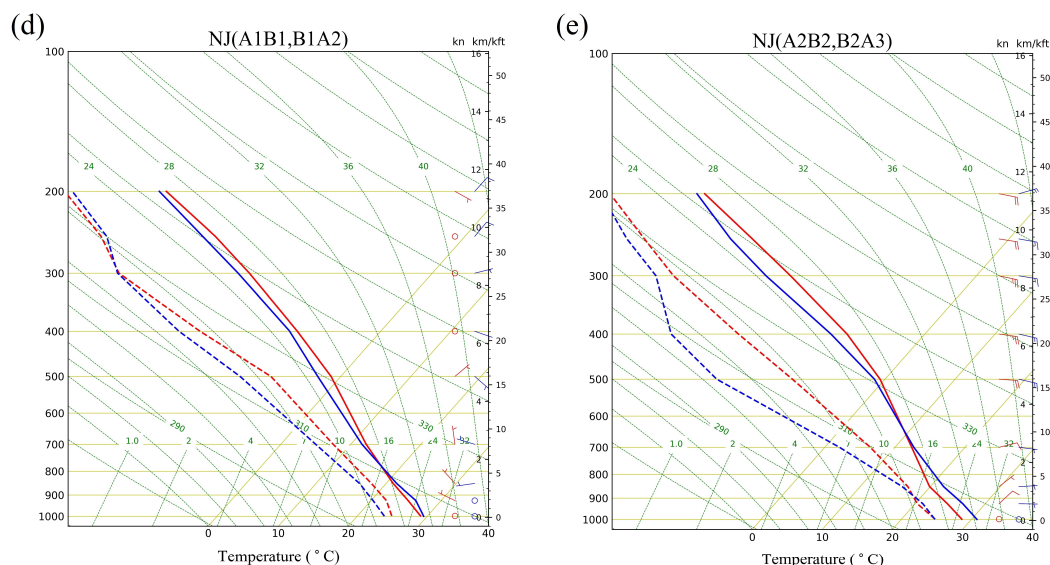
480



481



482



483

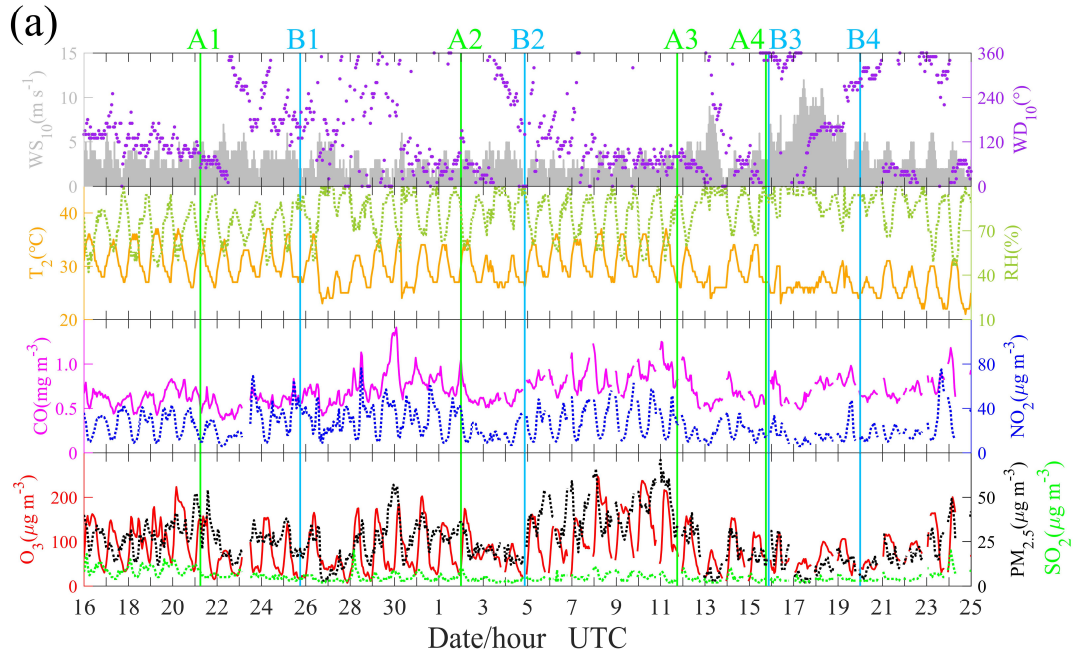
484 **Figure 9. Same as Figure 6, but for Nanjing.**

485

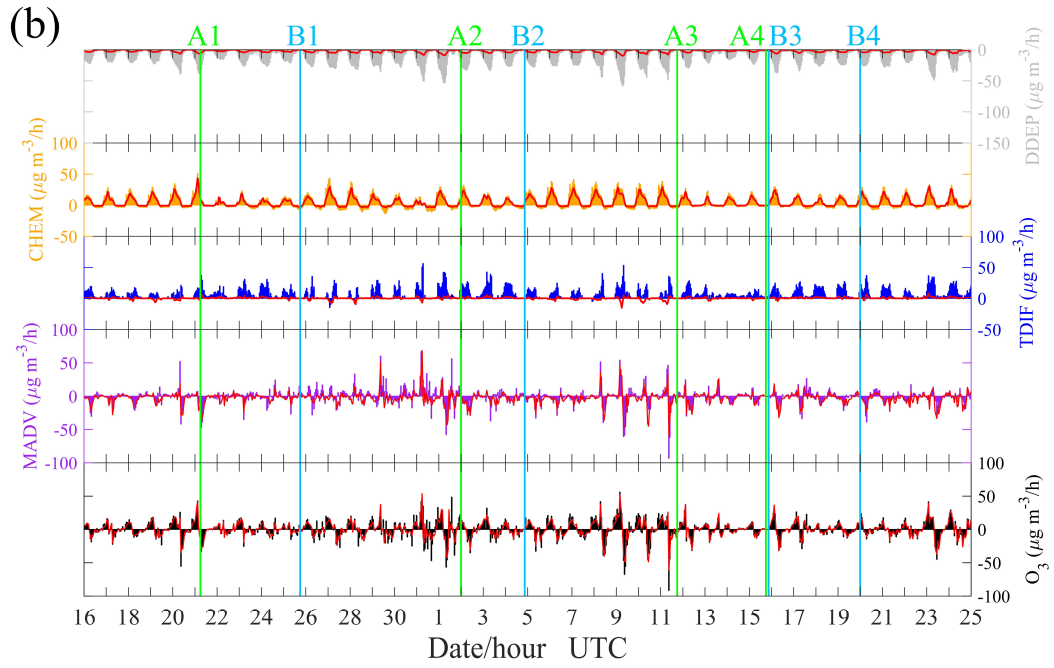
### 486 3.3.5 Hefei in category IV cities

487 Hefei is the city farthest from the coast among the four representative cities, and O<sub>3</sub> pollution  
 488 occurred on 31 July and 8-11 August. We also find the phenomenon that the precursors  
 489 concentrations had an increase once the wind direction changed from southeast to southwest (Figure  
 490 10a). During B1A2 and B2A3, the concentrations of the main precursors of O<sub>3</sub> was high. However,  
 491 high O<sub>3</sub> concentration was mainly found in B2A3, and not in B1A2. This may be related to the  
 492 relatively low temperature during B1A2 (Figure 10a), which is not conducive to photochemical  
 493 production of O<sub>3</sub> (Figure 10b). As shown in Figure 10c, there were distinct upward airflows within  
 494 the boundary layer, which may be related to urban effect (e.g., urban heat islands). These upward  
 495 airflows within the boundary layer help mix the air, resulting in a uniform distribution of O<sub>3</sub> in the  
 496 vertical direction. However, the downward airflows can still inhibit the vertical diffusion of O<sub>3</sub>, and  
 497 O<sub>3</sub> tends to be trapped within the boundary layer.

498

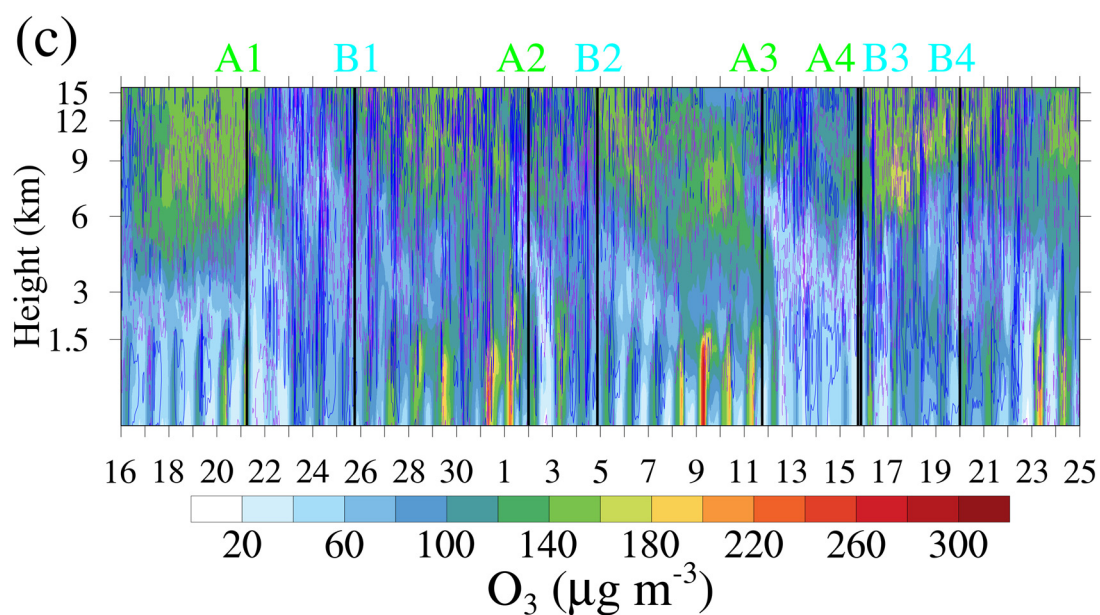


499



500





501

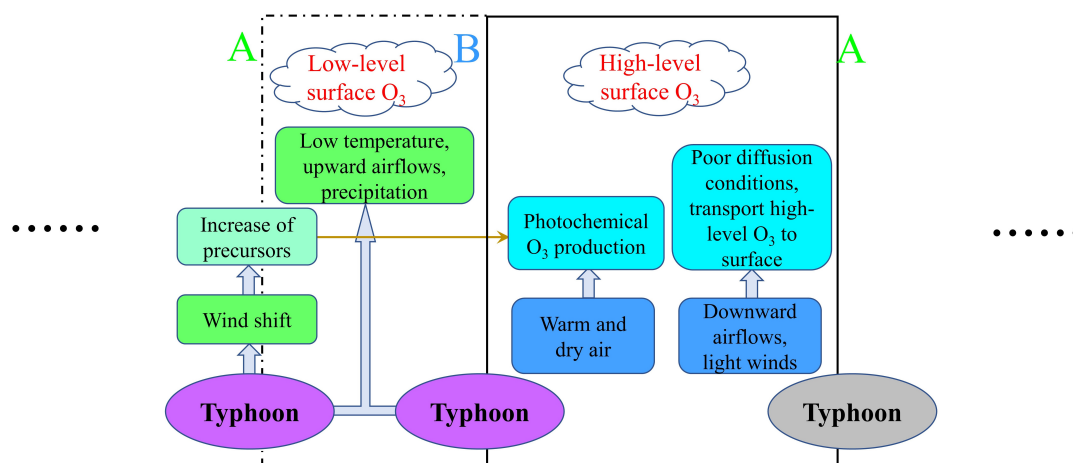
502 **Figure 10. Same as Figure 6 (a)-(c), but for Hefei.**

503

### 504 3.3.6 A schematic diagram of major processes

505 Although the processes of landfall typhoon affecting  $O_3$  varied from city to city, the major  
 506 processes have many similarities and can be summarized as a schematic diagram in Figure 11. The  
 507 YRD region, as a typical region of East Asian monsoon climate, is strongly influenced by typhoon  
 508 activities over the Western Pacific. In summer, the meteorological conditions of high temperature  
 509 and downward airflows combined with high levels of precursors due to the huge energy  
 510 consumption are all favorable to  $O_3$  accumulation in the region. However, powerful systems like  
 511 typhoon can break this state. For typhoons that may land in the YRD, by the time they approach the  
 512 24-hour warning line, the prevailing southeast wind in the YRD will change to southwest wind,  
 513 which can transport lots of precursors from inland to the YRD. The change in wind direction  
 514 depends on the track of the typhoon and the geographical location of cities, and often appears first  
 515 in cities along the coastline. With influence of a typhoon, the low temperature, precipitation (upward  
 516 airflows) and wild wind prevent high  $O_3$  and  $PM_{2.5}$  episodes from forming. Moreover, the effect of  
 517 removing pollutants is related to the intensity of typhoon landing, but some of the main precursors  
 518 of  $O_3$  are still at a high level due to foreign sources superposed with local emissions. After the  
 519 passing of typhoons, the atmosphere returns to a warm and dry state (even more so than before),

520 and the downward airflows resumed. The troposphere is then flooded with high O<sub>3</sub> due to two main  
 521 sources. One is that O<sub>3</sub>-rich air transported from the low stratosphere by the downward airflows,  
 522 and the other is that O<sub>3</sub> produced by strong photochemical reactions under the abundance of  
 523 precursors. O<sub>3</sub> is mainly generated inside the boundary layer (~1000 m) instead of at the surface.  
 524 The high-level O<sub>3</sub> can remain in the residual layer at night, and be transported to the surface by  
 525 downward airflows or turbulent mixing by the second day. At the same time, the wind readjusts to  
 526 southeast and wind speed is light, resulting in poor diffusion conditions. The downward airflows  
 527 and light wind obstruct the vertical and horizontal diffusion of O<sub>3</sub>, leaving O<sub>3</sub> trapped on the ground.  
 528 The thermal-dynamic effects result in high-level surface O<sub>3</sub> in the YRD.  
 529



530  
 531 **Figure 11. A schematic diagram of major processes that summertime O<sub>3</sub> is affected by landfall**  
 532 **typhoons in the YRD. The letter A indicates the moment that the typhoon has reached the 24-**  
 533 **h warning line, and letter B indicates the last moment when typhoon remains active in the**  
 534 **mainland China.**

535  
 536 Typhoon can exert an enormous impact on energy transports and air mass in the troposphere  
 537 as well as redistribution of pollutants. Though most typhoons generated over the western North  
 538 Pacific will not land in China, or they are more likely to land in the South China rather than the  
 539 YRD. In our previous study (Shu et al., 2016), the typhoon did not land in the YRD, but the  
 540 processes related to high-level O<sub>3</sub> formation may be the same. That is, the processes shown in the  
 541 open box enclosed by dashed lines in Figure 11, which are unique to landfall typhoons, while the

542 processes inside the box enclosed by solid lines can be found between typhoons. Transport of  
543 precursors, downward airflows, high temperature and light wind are crucial factors, and how big  
544 roles of those factors play in O<sub>3</sub> episodes depends on behaviors of the typhoons and geographical  
545 locations of the cities. Quantify these processes with just a few cases is a large challenge. For  
546 example, it is hard to find out whether the downward airflows are modulated by the subtropical high  
547 or the periphery circulation of typhoons since they usually occur simultaneously. Furthermore, the  
548 behave of particulate matter is intriguing since high-level PM<sub>2.5</sub> often occurs with high-level O<sub>3</sub>  
549 after typhoon, which is opposite to the suggestion that high particulate matter concentrations inhibit  
550 the formation of O<sub>3</sub> in previous studies (Li et al., 2005; Xing et al., 2017). This may be related to  
551 the heterogeneous reactions (Lou et al., 2014) but research on this issue is quite limited to date.

552

### 553 **3.3 Premature mortalities induced by O<sub>3</sub> exposure**

554 When it comes to typhoons, especially landfall typhoons, the first concern is the huge damage  
555 caused by extreme weathers. After the passing of typhoons, people are relieved and go back with  
556 their life as usual. However, our research indicates that high O<sub>3</sub> episodes are likely to occur in the  
557 short period after a typhoon landing in the YRD, and high O<sub>3</sub> concentrations can do harm to people's  
558 health. To arouse attention on this issue, we estimate the premature mortality attributed to O<sub>3</sub> for  
559 respiratory disease, we choose two complete cycles, which is the period A1A3 (21 July to 11 August),  
560 to do the calculation. In this study, we employ the standard damage function defined by  
561 epidemiology studies (Anenberg et al., 2010; Voorhees et al., 2014) to calculate the premature  
562 mortalities due to O<sub>3</sub> exposure, the specific formulas and parameters are described in Section 2.7.  
563 Table 4 summarized the premature mortalities in cities in the YRD. The premature mortalities are a  
564 function of both the population and O<sub>3</sub> levels, resulting in high premature mortalities in populated  
565 and heavily polluted areas. Out of the 26 cities in the YRD, Shanghai showed highest premature  
566 mortalities (29.2) due to its high surface O<sub>3</sub> concentrations and huge population. The city with the  
567 lowest premature mortalities (0.6) was Zhoushan, which may be related to removing effect of the  
568 maritime air masses as Zhoushan is located by the sea (Figure 1b). During this period, the total  
569 premature mortalities in the YRD was 194.0, which was larger than the number of casualties caused  
570 directly by the typhoons (80 people were killed by landfall typhoons in mainland China in 2018).

571

**Table 4. Premature mortalities induced by O<sub>3</sub> exposure for respiratory disease**

	City	Population (thousand)	Premature mortalities
Category I cities	Shanghai	24,240	29.2
	Yancheng	7,200	6.1
	Nantong	7,310	7.9
	Jiaxing	4,726	7.3
	Ningbo	8,202	8.1
	Zhoushan	1,173	0.6
	Taizhou	6,139	4.1
Category II cities	Hangzhou	9,806	16.5
	Taizhoushi	4,636	5.2
	Changzhou	4,729	4.4
	Wuxi	6,575	10.7
	Suzhou	10,722	15.3
	Huzhou	3,027	2.8
	Shaoxing	5,035	4.7
	Jinhua	5,604	8.2
Category III cities	Nanjing	8,436	13.4
	Yangzhou	4,531	5.5
	Zhenjiang	3,196	5.3
	Chuzhou	4,114	5.8
	Maanshan	2,337	3.6
	Wuhu	3,748	6.2
	Xuancheng	2,648	2.0
Category IV cities	Hefei	8,087	10.9
	Tongling	1,629	1.7
	Chizhou	1,475	2.1
	Anqing	4,691	6.4
<b>Total</b>		<b>154,016</b>	<b>194.0</b>

573

574 **4 Conclusions**

575 In this study, we investigate the detail processes of landfall typhoons affecting O<sub>3</sub> in the YRD  
576 based on a unique case from 16 July to 25 August, 2018, using both monitoring observations and  
577 numerical simulations. This case was characterized by two multiday regional O<sub>3</sub> pollution episodes  
578 involving four successive landfall typhoons. The two O<sub>3</sub> episodes appeared from 24 July to 2 August  
579 and 5 to 11 August, respectively, with the highest MDA8 O<sub>3</sub> reached up 264 µg m<sup>-3</sup>.

580 The time when a typhoon reaches the 24-h warning line and the time when the typhoon dies

581 away in the mainland China are crucial, because O<sub>3</sub> pollution episodes mainly occur during the  
582 period from the end of a typhoon to the arrival of the next typhoon in the YRD. These two moments  
583 can be roughly regarded as time nodes. Furthermore, it is found that the variations of O<sub>3</sub> was related  
584 to the track, duration and landing intensity of the typhoons during the study period. O<sub>3</sub> pollution  
585 first appeared in cities along the coastline along the track of the typhoons. The interval between two  
586 typhoons can affect the duration of high O<sub>3</sub> concentration in the YRD. Generally, sustained high O<sub>3</sub>  
587 concentration likely appeared in the region on days when the existing typhoon had dissipated before  
588 the arrival of the next one. Regarding the impact of the landing intensity of typhoon, the stronger  
589 the typhoon landed, the gale and precipitation accompanying the typhoon would be more effective  
590 in suppressing O<sub>3</sub> generation, resulting in lower O<sub>3</sub> concentration in the typhoon landing location.

591 The detail processes of landfall typhoons affecting O<sub>3</sub> depend on typhoons and cities. High  
592 temperature and downward airflows combined with abundant precursors are the main reasons for  
593 high O<sub>3</sub> concentration in the YRD in summer. And landfall typhoons can change this state through  
594 the following mechanism: When the landfall typhoon is close enough (~ 24-hour warning line), the  
595 prevailing southeast wind will change to southwest wind, which transports large amount of  
596 precursors from inland to the YRD. The southwest wind usually appears first in coastal regions, and  
597 the wind direction will turn to southeast as long as the YRD is dominated by the subtropical high.  
598 Then the typhoon makes landfall, the low temperature, precipitation (upward airflows) and wild  
599 wind suppress the generation of O<sub>3</sub>. After the typhoon passing, the atmosphere in low layers (below  
600 700 hPa) will be warm and dry, and downward airflows resume. The troposphere is likely to fill  
601 with high concentration of O<sub>3</sub> due to O<sub>3</sub>-rich air transported from the low stratosphere and strong  
602 photochemical reactions. O<sub>3</sub> is mainly generated in the middle of boundary layer (~ 1000 m) instead  
603 of at the surface. The high-level O<sub>3</sub> can remain in the residual layer at night, and can be transported  
604 to the surface by downward airflows or turbulent mixing by the second day. The downward airflows  
605 also obstruct the vertical diffusion of O<sub>3</sub>. Meanwhile, wind speed is light when the wind readjusts  
606 to southeast, which further reduces horizontal diffusion of O<sub>3</sub>. Thus, O<sub>3</sub> can be accumulated and  
607 trapped on the ground. The thermal-dynamic effects results in high surface O<sub>3</sub> concentration in the  
608 YRD. Those processes will repeat if the next typhoon approaches.

609 The estimated premature mortalities attributed to O<sub>3</sub> exposure for respiratory disease in the  
610 YRD during 21 July to 11 August (two complete cycles of typhoons) was 194.0, which is larger

611 than the number of casualties caused directly by the typhoons. This work has enhanced our  
612 understanding of how landfall typhoons affect O<sub>3</sub> in the YRD, which may help synthetically forecast  
613 O<sub>3</sub> pollution modulated by the subtropical high and typhoons. Meanwhile, our results further  
614 confirm that large-scale synoptic weather systems play an important role in regional air pollution,  
615 suggesting a need in establishing potential links between air pollution and predominant synoptic  
616 weather patterns.

617

618 **Author contributions.** C. C. Zhan and M. Xie had the original ideas, designed the research, collected  
619 the data, and prepared the original draft. C. C. Zhan carried out the data analysis. M. Xie acquired  
620 financial support for the project leading to this publication. C. W. Huang taught and helped C. C.  
621 Zhan to do the numerical simulation. T. J. Wang and J. Liu revised the manuscript and helped to  
622 collect the data. C. Q. Ma helped to deal with the emission inventory. M. Xu and J. W. Yu helped to  
623 collect the data. M. M. Li, S. Li, B. L. Zhuang, and M. Zhao reviewed the initial draft and checked  
624 the English of the original manuscript. Y. M. Jiao and D. Y. Nie reviewed the initial draft and helped  
625 to improve the work of health impact.

626

627 **Acknowledgements.**

628 This work was supported by the National Key Research and Development Program of China  
629 (2018YFC0213502, 2018YFC1506404), the open research fund of Chongqing Meteorological  
630 Bureau (KFJJ-201607) and the Fundamental Research Funds for the Central Universities  
631 (020714380047).

632

### 633 **References**

634 Allen, R. J., Sherwood, S. C., Norris, J. R., and Zender, C. S.: Recent Northern Hemisphere tropical  
635 expansion primarily driven by black carbon and tropospheric ozone, *Nature*, 485, 350-354,  
636 10.1038/nature11097, 2012.

637 Anenberg, S. C., Horowitz, L. W., Tong, D. Q., and West, J. J.: An estimate of the global burden of  
638 anthropogenic ozone and fine particulate matter on premature human mortality using  
639 atmospheric modeling, *Environ Health Perspect*, 118, 1189-1195, 10.1289/ehp.0901220, 2010.

640 Burnett, R. T., Pope, C. A., 3rd, Ezzati, M., Olives, C., Lim, S. S., Mehta, S., Shin, H. H., Singh, G.,

641 Hubbell, B., Brauer, M., Anderson, H. R., Smith, K. R., Balmes, J. R., Bruce, N. G., Kan, H.,  
642 Laden, F., Pruss-Ustun, A., Turner, M. C., Gapstur, S. M., Diver, W. R., and Cohen, A.: An  
643 integrated risk function for estimating the global burden of disease attributable to ambient fine  
644 particulate matter exposure, *Environ Health Perspect*, 122, 397-403, 10.1289/ehp.1307049,  
645 2014.

646 Chameides, W., and Walker, J. C. G.: A photochemical theory of tropospheric ozone, *Journal of*  
647 *Geophysical Research*, 78, 8751-8760, 10.1029/JC078i036p08751, 1973.

648 Chan, C. K., and Yao, X.: Air pollution in mega cities in China, *Atmospheric Environment*, 42, 1-  
649 42, 10.1016/j.atmosenv.2007.09.003, 2008.

650 Deng, T., Wang, T., Wang, S., Zou, Y., Yin, C., Li, F., Liu, L., Wang, N., Song, L., Wu, C., and Wu,  
651 D.: Impact of typhoon periphery on high ozone and high aerosol pollution in the Pearl River  
652 Delta region, *The Science of the total environment*, 668, 617-630,  
653 10.1016/j.scitotenv.2019.02.450, 2019.

654 Ding, A. J., Wang, T., Thouret, V., Cammas, J. P., and Nedelec, P.: Tropospheric ozone climatology  
655 over Beijing: analysis of aircraft data from the MOZAIC program, *Atmospheric Chemistry and*  
656 *Physics*, 8, 1-13, 2008.

657 Ding, A. J., Fu, C. B., Yang, X. Q., Sun, J. N., Zheng, L. F., Xie, Y. N., Herrmann, E., Nie, W., Petäjä,  
658 T., Kerminen, V. M., and Kulmala, M.: Ozone and fine particle in the western Yangtze River  
659 Delta: an overview of 1 yr data at the SORPES station, *Atmospheric Chemistry and Physics*,  
660 13, 5813-5830, 10.5194/acp-13-5813-2013, 2013.

661 Ding, A., Nie, W., Huang, X., Chi, X., Sun, J., Kerminen, V.-M., Xu, Z., Guo, W., Petäjä, T., Yang,  
662 X., Kulmala, M., and Fu, C.: Long-term observation of air pollution-weather/climate  
663 interactions at the SORPES station: a review and outlook, *Frontiers of Environmental Science*  
664 *& Engineering*, 10, 10.1007/s11783-016-0877-3, 2016.

665 Dong J Y, Liu X R, Zhang B Z.: Meta-analysis of association between short-term ozone exposure  
666 and population mortality in China, *Acta Scientiae Circumstantiae*, 36 (4), 1477-1485, 2016 (in  
667 Chinese).

668 Fan, Q., Lan, J., Liu, Y. M., Wang, X. M., Chan, P. W., Hong, Y. Y., Feng, Y. R., Liu, Y. X., Zeng, Y.  
669 J., and Liang, G. X.: Process analysis of regional aerosol pollution during spring in the Pearl  
670 River Delta region, China, *Atmospheric Environment*, 122, 829-838, 2015.

671 Ghude, S. D., Chate, D. M., Jena, C., Beig, G., Kumar, R., Barth, M. C., Pfister, G. G., Fadnavis, S.,  
672 and Pithani, P.: Premature mortality in India due to PM<sub>2.5</sub> and ozone exposure, *Geophys Res*  
673 *Lett*, 43, 4650-4658, 10.1002/2016gl068949, 2016.

674 Guo, S., Hu, M., Zamora, M. L., Peng, J., Shang, D., Zheng, J., Du, Z., Wu, Z., Shao, M., Zeng, L.,  
675 Molina, M. J., and Zhang, R.: Elucidating severe urban haze formation in China, *Proceedings*  
676 *of the National Academy of Sciences of the United States of America*, 111, 17373-17378,  
677 10.1073/pnas.1419604111, 2014.

678 Hu, J., Chen, J., Ying, Q., and Zhang, H.: One-year simulation of ozone and particulate matter in  
679 China using WRF/CMAQ modeling system, *Atmospheric Chemistry and Physics*, 16, 10333-  
680 10350, 10.5194/acp-16-10333-2016, 2016.

681 Huang, J.-P.: Numerical simulation and process analysis of typhoon-related ozone episodes in Hong  
682 Kong, *Journal of Geophysical Research*, 110, 10.1029/2004jd004914, 2005.

683 Huang, R. J., Zhang, Y., Bozzetti, C., Ho, K. F., Cao, J. J., Han, Y., Daellenbach, K. R., Slowik, J.  
684 G., Platt, S. M., Canonaco, F., Zotter, P., Wolf, R., Pieber, S. M., Bruns, E. A., Crippa, M.,  
685 Ciarelli, G., Piazzalunga, A., Schwikowski, M., Abbaszade, G., Schnelle-Kreis, J.,  
686 Zimmermann, R., An, Z., Szidat, S., Baltensperger, U., El Haddad, I., and Prevot, A. S.: High  
687 secondary aerosol contribution to particulate pollution during haze events in China, *Nature*,  
688 514, 218-222, 10.1038/nature13774, 2014.

689 Jerrett, M., Burnett, R. T., Pope, C. A., Ito, K., Thurston, G., Krewski, D., Shi, Y. L., Calle, E., and  
690 Thun, M.: Long-Term Ozone Exposure and Mortality., *New Engl J Med*, 360, 1085-1095, 2009.

691 Jiang, Y. C., Zhao, T. L., Liu, J., Xu, X. D., Tan, C. H., Cheng, X. H., Bi, X. Y., Gan, J. B., You, J.  
692 F., and Zhao, S. Z.: Why does surface ozone peak before a typhoon landing in southeast China?,  
693 *Atmospheric Chemistry and Physics*, 15, 13331-13338, 10.5194/acp-15-13331-2015, 2015.

694 Jiménez, P. A., and Dudhia, J.: Improving the Representation of Resolved and Unresolved  
695 Topographic Effects on Surface Wind in the WRF Model, *Journal of Applied Meteorology and*  
696 *Climatology*, 51, 300-316, 10.1175/jamc-d-11-084.1, 2012.

697 Jin, Y., Andersson, H., and Zhang, S.: Air Pollution Control Policies in China: A Retrospective and  
698 Prospects, *Int J Environ Res Public Health*, 13, 10.3390/ijerph13121219, 2016.

699 Kamens, R., Jang, M., Chien, C. J., and Leach, K.: Aerosol formation from the reaction of alpha-  
700 pinene and ozone using a gas-phase kinetics aerosol partitioning model, *Environmental*



701 Science & Technology, 33, 1430-1438, 1999.

702 Kan, H., Chen, R., and Tong, S.: Ambient air pollution, climate change, and population health in  
703 China, *Environ Int*, 42, 10-19, 10.1016/j.envint.2011.03.003, 2012.

704 Khoder, M. I.: Atmospheric conversion of sulfur dioxide to particulate sulfate and nitrogen dioxide  
705 to particulate nitrate and gaseous nitric acid in an urban area, *Chemosphere*, 49, 675-684, 2002.

706 Lelieveld, J., Evans, J. S., Fnais, M., Giannadaki, D., and Pozzer, A.: The contribution of outdoor  
707 air pollution sources to premature mortality on a global scale, *Nature*, 525, 367-371,  
708 10.1038/nature15371, 2015.

709 Li, L., Chen, C. H., Fu, J. S., Huang, C., Streets, D. G., Huang, H. Y., Zhang, G. F., Wang, Y. J.,  
710 Jang, C. J., Wang, H. L., Chen, Y. R., and Fu, J. M.: Air quality and emissions in the Yangtze  
711 River Delta, China, *Atmospheric Chemistry and Physics*, 11, 1621-1639, 10.5194/acp-11-  
712 1621-2011, 2011.

713 Li, L., Chen, C. H., Huang, C., Huang, H. Y., Zhang, G. F., Wang, Y. J., Wang, H. L., Lou, S. R.,  
714 Qiao, L. P., Zhou, M., Chen, M. H., Chen, Y. R., Streets, D. G., Fu, J. S., and Jang, C. J.: Process  
715 analysis of regional ozone formation over the Yangtze River Delta, China using the Community  
716 Multi-scale Air Quality modeling system, *Atmospheric Chemistry and Physics*, 12, 10971-  
717 10987, 2012.

718 Li, S. H., and Hong, H. P.: Typhoon wind hazard estimation for China using an empirical track  
719 model, *Natural Hazards*, 82, 1009-1029, 10.1007/s11069-016-2231-2, 2016.

720 Li, M., Liu, H., Geng, G., Hong, C., Liu, F., Song, Y., Tong, D., Zheng, B., Cui, H., Man, H., Zhang,  
721 Q., and He, K.: Anthropogenic emission inventories in China: a review, *National Science*  
722 *Review*, 4, 834-866, 10.1093/nsr/nwx150, 2017.

723 Li, M., Wang, T., Xie, M., Zhuang, B., Li, S., Han, Y., and Chen, P.: Impacts of aerosol-radiation  
724 feedback on local air quality during a severe haze episode in Nanjing megacity, eastern China,  
725 *Tellus B: Chemical and Physical Meteorology*, 69, 10.1080/16000889.2017.1339548, 2017.

726 Li, M., Wang, T., Xie, M., Zhuang, B., Li, S., Han, Y., Song, Y., and Cheng, N.: Improved  
727 meteorology and ozone air quality simulations using MODIS land surface parameters in the  
728 Yangtze River Delta urban cluster, China, *Journal of Geophysical Research: Atmospheres*, 122,  
729 3116-3140, 10.1002/2016jd026182, 2017.

730 Li, S., Wang, T., Huang, X., Pu, X., Li, M., Chen, P., Yang, X.-Q., and Wang, M.: Impact of East

731 Asian Summer Monsoon on Surface Ozone Pattern in China, *Journal of Geophysical Research:*  
732 *Atmospheres*, 123, 1401-1411, 10.1002/2017jd027190, 2018.

733 Li, M., Wang, T., Xie, M., Li, S., Zhuang, B., Huang, X., Chen, P., Zhao, M., and Liu, J.: Formation  
734 and Evolution Mechanisms for Two Extreme Haze Episodes in the Yangtze River Delta Region  
735 of China During Winter 2016, *Journal of Geophysical Research: Atmospheres*, 124, 3607-3623,  
736 10.1029/2019jd030535, 2019.

737 Liao, J., Wang, T., Jiang, Z., Zhuang, B., Xie, M., Yin, C., Wang, X., Zhu, J., Fu, Y., and Zhang, Y.:  
738 WRF/Chem modeling of the impacts of urban expansion on regional climate and air pollutants  
739 in Yangtze River Delta, China, *Atmospheric Environment*, 106, 204-214,  
740 10.1016/j.atmosenv.2015.01.059, 2015.

741 Liao, Z., Gao, M., Sun, J., and Fan, S.: The impact of synoptic circulation on air quality and  
742 pollution-related human health in the Yangtze River Delta region, *The Science of the total*  
743 *environment*, 607-608, 838-846, 10.1016/j.scitotenv.2017.07.031, 2017.

744 Liu, D., Pang, L., and Xie, B.: Typhoon disaster in China: prediction, prevention, and mitigation,  
745 *Natural Hazards*, 49, 421-436, 10.1007/s11069-008-9262-2, 2009.

746 Liu, H., Liu, S., Xue, B. R., Lv, Z. F., Meng, Z. H., Yang, X. F., Xue, T., Yu, Q., and He, K. B.:  
747 Ground-level ozone pollution and its health impacts in China, *Atmospheric Environment*, 173,  
748 223-230, 2018.

749 Lou, S., Liao, H., and Zhu, B.: Impacts of aerosols on surface-layer ozone concentrations in China  
750 through heterogeneous reactions and changes in photolysis rates, *Atmospheric Environment*,  
751 85, 123-138, 10.1016/j.atmosenv.2013.12.004, 2014.

752 Lu, X., Hong, J., Zhang, L., Cooper, O. R., Schultz, M. G., Xu, X., Wang, T., Gao, M., Zhao, Y., and  
753 Zhang, Y.: Severe Surface Ozone Pollution in China: A Global Perspective, *Environmental*  
754 *Science & Technology Letters*, 5, 487-494, 10.1021/acs.estlett.8b00366, 2018.

755 Monks, P. S., Archibald, A. T., Colette, A., Cooper, O., Coyle, M., Derwent, R., Fowler, D., Granier,  
756 C., Law, K. S., Mills, G. E., Stevenson, D. S., Tarasova, O., Thouret, V., von Schneidmesser,  
757 E., Sommariva, R., Wild, O., and Williams, M. L.: Tropospheric ozone and its precursors from  
758 the urban to the global scale from air quality to short-lived climate forcer, *Atmospheric*  
759 *Chemistry and Physics*, 15, 8889-8973, 10.5194/acp-15-8889-2015, 2015.

760 Shu, L., Xie, M., Wang, T., Gao, D., Chen, P., Han, Y., Li, S., Zhuang, B., and Li, M.: Integrated

761 studies of a regional ozone pollution synthetically affected by subtropical high and typhoon  
762 system in the Yangtze River Delta region, China, *Atmospheric Chemistry and Physics*, 16,  
763 15801-15819, 10.5194/acp-16-15801-2016, 2016.

764 Shu, L., Xie, M., Gao, D., Wang, T., Fang, D., Liu, Q., Huang, A., and Peng, L.: Regional severe  
765 particle pollution and its association with synoptic weather patterns in the Yangtze River Delta  
766 region, China, *Atmospheric Chemistry and Physics*, 17, 12871-12891, 10.5194/acp-17-12871-  
767 2017, 2017.

768 Tang, X.Y., Li, J.L., Dong, Z.X., Wang, Y.Y., Wang, W.X., Qi, L.W., Liu, X.L., Zhang, Y.T., Zhang,  
769 X.J., Tian, B.S., Jin, S.W., Yang, L.Q., Zhang, Y.X., 1989. Photochemical pollution in Lanzhou,  
770 China - a case study. *J. Environ. Sci. China* 1, 31e38.

771 Van Dingenen, R., Dentener, F. J., Raes, F., Krol, M. C., Emberson, L., and Cofala, J.: The global  
772 impact of ozone on agricultural crop yields under current and future air quality legislation,  
773 *Atmospheric Environment*, 43, 604-618, 10.1016/j.atmosenv.2008.10.033, 2009.

774 Voorhees, A. S., Wang, J., Wang, C., Zhao, B., Wang, S., and Kan, H.: Public health benefits of  
775 reducing air pollution in Shanghai: a proof-of-concept methodology with application to  
776 BenMAP, *The Science of the total environment*, 485-486, 396-405,  
777 10.1016/j.scitotenv.2014.03.113, 2014.

778 Wang, T., and Kwok, J. Y. H.: Measurement and analysis of a multiday photochemical smog episode  
779 in the Pearl River delta of China, *J Appl Meteorol*, 42, 404-416, 2003.

780 Wang, X., Zhang, Y., Hu, Y., Zhou, W., Lu, K., Zhong, L., Zeng, L., Shao, M., Hu, M., and Russell,  
781 A. G.: Process analysis and sensitivity study of regional ozone formation over the Pearl River  
782 Delta, China, during the PRIDE-PRD2004 campaign using the Community Multiscale Air  
783 Quality modeling system, *Atmospheric Chemistry and Physics*, 10, 4423-4437, 10.5194/acp-  
784 10-4423-2010, 2010.

785 Wang, M., Cao, C., Li, G., and Singh, R. P.: Analysis of a severe prolonged regional haze episode  
786 in the Yangtze River Delta, China, *Atmospheric Environment*, 102, 112-121,  
787 10.1016/j.atmosenv.2014.11.038, 2015.

788 Wang, T., Xue, L., Brimblecombe, P., Lam, Y. F., Li, L., and Zhang, L.: Ozone pollution in China:  
789 A review of concentrations, meteorological influences, chemical precursors, and effects, *The  
790 Science of the total environment*, 575, 1582-1596, 10.1016/j.scitotenv.2016.10.081, 2017.

791 Wang, T., Gao, T., Zhang, H., Ge, M., Lei, H., Zhang, P., Zhang, P., Lu, C., Liu, C., Zhang, H.,  
792 Zhang, Q., Liao, H., Kan, H., Feng, Z., Zhang, Y., Qie, X., Cai, X., Li, M., Liu, L., and Tong,  
793 S.: Review of Chinese atmospheric science research over the past 70 years: Atmospheric  
794 physics and atmospheric environment, *Science China Earth Sciences*, 62, 1903-1945,  
795 10.1007/s11430-019-9536-1, 2019.

796 Wei, X., Lam, K.-s., Cao, C., Li, H., and He, J.: Dynamics of the Typhoon Haitang Related High  
797 Ozone Episode over Hong Kong, *Advances in Meteorology*, 2016, 1-12,  
798 10.1155/2016/6089154, 2016.

799 Xie, M., Zhu, K., Wang, T., Yang, H., Zhuang, B., Li, S., Li, M., Zhu, X., and Ouyang, Y.:  
800 Application of photochemical indicators to evaluate ozone nonlinear chemistry and pollution  
801 control countermeasure in China, *Atmospheric Environment*, 99, 466-473,  
802 10.1016/j.atmosenv.2014.10.013, 2014.

803 Xie, M., Liao, J., Wang, T., Zhu, K., Zhuang, B., Han, Y., Li, M., and Li, S.: Modeling of the  
804 anthropogenic heat flux and its effect on regional meteorology and air quality over the Yangtze  
805 River Delta region, China, *Atmospheric Chemistry and Physics*, 16, 6071-6089, 10.5194/acp-  
806 16-6071-2016, 2016.

807 Xie, M., Zhu, K., Wang, T., Chen, P., Han, Y., Li, S., Zhuang, B., and Shu, L.: Temporal  
808 characterization and regional contribution to O<sub>3</sub> and NO<sub>x</sub> at an urban and a suburban site in  
809 Nanjing, China, *The Science of the total environment*, 551-552, 533-545,  
810 10.1016/j.scitotenv.2016.02.047, 2016.

811 Xie, M., Shu, L., Wang, T.-j., Liu, Q., Gao, D., Li, S., Zhuang, B.-l., Han, Y., Li, M.-m., and Chen,  
812 P.-l.: Natural emissions under future climate condition and their effects on surface ozone in the  
813 Yangtze River Delta region, China, *Atmospheric Environment*, 150, 162-180,  
814 10.1016/j.atmosenv.2016.11.053, 2017.

815 Xu, X., Lin, W., Wang, T., Yan, P., Tang, J., Meng, Z., and Wang, Y.: Long-term trend of surface  
816 ozone at a regional background station in eastern China 1991-2006: enhanced variability,  
817 *Atmospheric Chemistry and Physics*, 8, 2595-2607, 2008.

818 Xue, L. K., Wang, T., Gao, J., Ding, A. J., Zhou, X. H., Blake, D. R., Wang, X. F., Saunders, S. M.,  
819 Fan, S. J., Zuo, H. C., Zhang, Q. Z., and Wang, W. X.: Ground-level ozone in four Chinese  
820 cities: precursors, regional transport and heterogeneous processes, *Atmospheric Chemistry and*

821 Physics, 14, 13175-13188, 10.5194/acp-14-13175-2014, 2014.

822 Yang, J. X., Lau, A. K. H., Fung, J. C. H., Zhou, W., and Wenig, M.: An air pollution episode and  
823 its formation mechanism during the tropical cyclone Nuri's landfall in a coastal city of south  
824 China, *Atmospheric Environment*, 54, 746-753, 10.1016/j.atmosenv.2011.12.023, 2012.

825 Ying, M., Zhang, W., Yu, H., Lu, X., Feng, J., Fan, Y., Zhu, Y., and Chen, D.: An Overview of the  
826 China Meteorological Administration Tropical Cyclone Database, *Journal of Atmospheric and*  
827 *Oceanic Technology*, 31, 287-301, 10.1175/jtech-d-12-00119.1, 2014.

828 Zhan, C.-c., Xie, M., Fang, D.-x., Wang, T.-j., Wu, Z., Lu, H., Li, M.-m., Chen, P.-l., Zhuang, B.-l.,  
829 Li, S., Zhang, Z.-q., Gao, D., Ren, J.-y., and Zhao, M.: Synoptic weather patterns and their  
830 impacts on regional particle pollution in the city cluster of the Sichuan Basin, China,  
831 *Atmospheric Environment*, 208, 34-47, 10.1016/j.atmosenv.2019.03.033, 2019.

832 Zhang, Q. A., Wu, L. G., and Liu, Q. F.: Tropical Cyclone Damages in China 1983-2006, *Bulletin*  
833 *of the American Meteorological Society*, 90, 489-+, 2009.

834 Zhao, C., Wang, Y., Yang, Q., Fu, R., Cunnold, D., and Choi, Y.: Impact of East Asian summer  
835 monsoon on the air quality over China: View from space, *Journal of Geophysical Research*,  
836 115, 10.1029/2009jd012745, 2010.

837 Zhao, K., Li, X., Xue, M., Jou, B. J.-D., and Lee, W.-C.: Short-term forecasting through intermittent  
838 assimilation of data from Taiwan and mainland China coastal radars for Typhoon Meranti  
839 (2010) at landfall, *Journal of Geophysical Research: Atmospheres*, 117, n/a-n/a,  
840 10.1029/2011jd017109, 2012.

841